



This is a post-peer-review, pre-copyedit version of an article published in PNAS. Proceedings of the National Academy of Sciences. The original publication is available at: <https://doi.org/10.1073/pnas.2019346118>

Full citation reference:

Chauvigné, François, Carla Ducat, Alba Ferré, Tom Hansen, Montserrat Carrascal, Joaquín Abián, Roderick Nigel Finn, and Joan Cerdà. 2021. "A Multiplier Peroxiporin Signal Transduction Pathway Powers Piscine Spermatozoa". *Proceedings Of The National Academy Of Sciences* 118 (10): e2019346118. doi:10.1073/pnas.2019346118.

Document downloaded from:



1 CLASSIFICATION: BIOLOGICAL SCIENCES, PHYSIOLOGY

2
3 **A multiplier peroxiporin signal transduction pathway**
4 **powers piscine spermatozoa**

5
6 **François Chauvigné^a, Carla Ducat^a, Alba Ferré^a, Tom Hansen^c, Montserrat**
7 **Carrascal^d, Joaquín Abián^d, Roderick Nigel Finn^{a,b} and Joan Cerdà^{a,1}**

8
9 ^aIRTA-Institute of Biotechnology and Biomedicine (IBB), Universitat Autònoma de Barcelona, 08193
10 Barcelona, Spain.

11 ^bDepartment of Biology, Bergen High Technology Centre, University of Bergen, 5020 Bergen, Norway.

12 ^cInstitute of Marine Research, Nordnes, 5817 Bergen, Norway.

13 ^dCSIC/UAB Proteomics Laboratory, IIBB-CSIC-IDIBAPS, Universitat Autònoma de Barcelona, 08193
14 Barcelona, Spain.

15
16 **The primary task of a spermatozoon is to deliver its nuclear payload to the egg to**
17 **form the next generation zygote. With polyandry repeatedly evolving in the animal**
18 **kingdom, however, sperm competition has become widespread, with the highest**
19 **known intensities occurring in fish. Yet, the molecular controls regulating**
20 **spermatozoon swimming performance in these organisms are largely unknown.**
21 **Here, we show that the kinematic properties of post-activated piscine spermatozoa**
22 **are regulated through a conserved trafficking mechanism whereby a peroxiporin**
23 **ortholog of mammalian aquaporin-8 (Aqp8bb) is inserted into the inner**
24 **mitochondrial membrane to facilitate H₂O₂ efflux in order to maintain ATP**
25 **production. In teleosts from more ancestral lineages, such as the zebrafish (*Danio***
26 ***rerio*) and the Atlantic salmon (*Salmo salar*), in which spermatozoa are activated in**
27 **freshwater, an intracellular Ca²⁺-signalling directly regulates this mechanism**
28 **through monophosphorylation of the Aqp8bb N-terminus. By contrast, in more**
29 **recently evolved marine teleosts, such the gilthead seabream (*Sparus aurata*), in**
30 **which spermatozoa activation occurs in seawater, a cross talk between Ca²⁺- and**
31 **oxidative stress-activated pathways generate a multiplier regulation of channel**
32 **trafficking via dual N-terminal phosphorylation. These findings reveal that teleost**
33 **spermatozoa evolved increasingly sophisticated detoxification pathways to**
34 **maintain swimming performance under a high osmotic stress, and provide novel**
35 **insight into molecular traits that are advantageous for post-copulatory sexual**
36 **selection.**

37
38 **Keywords:** aquaporin, mitochondria, osmotic stress, oxidative stress, sperm, fertility,
39 sexual selection, sperm competition

40
41 Author contributions: J.C and F.C designed research; F.C., C.D., A.F., and T.H.
42 performed research; J.A., M.C. and T.H. contributed new reagents/analytic tools; J.C.,
43 F.C and R.N.F. analyzed data; and F.C., R.N.F. and J.C. wrote the paper.

44
45 The authors declare no competing interest.

46
47 ¹To whom correspondence may be addressed. Email: joan.cerda@irta.cat

48
49 This article contains supporting information.

51 **Significance statement**

52

53 Spermatozoon swimming performance is critical for fertilisation success in fishes, yet
54 the cellular mechanisms that regulate this vital trait are poorly understood. Here, we
55 discovered that a water channel protein, acting as an H₂O₂ channel (peroxiporin) to
56 detoxify the mitochondria, directly regulates the velocity and progressive motility of
57 both freshwater and marine spermatozoa. The mitochondrial insertion of the peroxiporin
58 is controlled by an increasingly sophisticated hierarchy of intracellular signalling
59 cascades, which evolved into a multiplier stress-activated pathway in modern marine
60 species. These adaptive solutions maximize the post-activated swimming performance
61 of sperm under conditions of high osmotic and oxidative stress. Our findings thus reveal
62 that the pathways regulating the peroxiporin transport in fish spermatozoa provide an
63 advantage for competitive fertilization success.

64

65 Introduction

66

67 For many dioecious animals, spermatozoon velocity, progressivity and duration of
68 motility are vital determinants of reproductive success and are thus major selection
69 criteria for sperm evolution (1-6). Maximising such kinematic properties contributes to
70 spermatozoon vigour (7), however, due to the limitations in sperm ATP stores, which
71 provide the chemical energy for flagellar contractions, a trade-off between swimming
72 fast and for extended periods typically exists (8). Optimal combinations of traits that
73 improve spermatozoon vigour are nevertheless important in polyandrous vertebrates
74 facing sperm competition, which represents a powerful form of post-copulatory sexual
75 selection (9-15). Since the phenomenon of sperm competition was first recognised (16),
76 investigators have sought to understand the underlying mechanisms that could explain
77 advantageous trait selection (17). To date, however, most research has focused on the
78 physical and morphological properties involved in sperm competition, and very little is
79 known concerning the molecular and genetic mechanisms underpinning spermatozoon
80 performance (15, 18, 19).

81 One positively selected morphological change in respect of spermatozoon velocity
82 and longevity in vertebrates as diverse as fishes, birds and mammals, has been the
83 increase in the spermatozoon midpiece size and the number or scale of mitochondria
84 therein (20-22). Such changes have logically been associated with increased
85 mitochondrial production of ATP for improved flagellar motility. However, the
86 biochemical reactions that lead to increased ATP synthesis also generate elevated levels
87 of hydrogen peroxide (H_2O_2), a reactive oxygen species (ROS) that inhibits
88 mitochondrial function and suppresses flagellar motility (23-27). With osmotic stress of
89 the exposed ejaculate generating additional ROS (26, 28), it has been unclear how
90 sperm evolved molecular mechanisms that surmount such signaling conflicts.

91 A solution to this apparent paradox was recently discovered in the spermatozoa of
92 a marine teleost, in which a water channel protein, now termed Aqp8bb (29), is rapidly
93 (< 1 sec) trafficked to the inner mitochondrial membrane upon activation in seawater
94 (SW) to facilitate H_2O_2 efflux and the maintenance of ATP production and flagellar
95 motility (26). The importance of Aqp8bb, which mainly functions as a peroxiporin in
96 these germ cells, was demonstrated through immunological inhibitory experiments,
97 which highlighted the channel trafficking mechanism as a critical regulator of the
98 spermatozoon velocity and motility (26). To date, however, the signal transduction
99 pathways that regulate peroxiporin trafficking in vertebrate spermatozoa remain
100 completely unknown.

101 Amongst externally fertilizing vertebrates, the highest known intensity of sperm
102 competition occurs in true bony fishes (teleosts) (6), and we therefore focused our
103 investigations on these model organisms. In contrast to amniotic vertebrates, in which
104 ejaculates become gelatinous when emitted (30), the ejaculates of freshwater (FW) and
105 marine teleosts are not only rapidly diluted, but respectively face tremendous and
106 opposing osmotic stresses, which in most species activate sperm motility (31-33). To
107 understand the significance of such harsh environments for peroxiporin signal
108 transduction pathway evolution, we selected model species from ancient and modern
109 lineages of teleosts, including the FW ostariphsyan zebrafish (*Danio rerio*), the FW
110 protacanthopterygian Atlantic salmon (*Salmo salar*) and the modern marine
111 acanthomorph gilthead seabream (*Sparus aurata*). Using a combination of
112 pharmacological, molecular and physiological approaches, we uncover the evolution of
113 increasingly sophisticated peroxiporin signal transduction pathways powering their
114 spermatozoa. The findings provide new insight into the underlying hierarchy of

115 systemic molecular traits that regulate the velocity, progressivity and duration of
116 spermatozoon motility.

117

118 **Results**

119

120 **Activated piscine spermatozoa traffic the Aqp8bb peroxiporin to mitochondria.** To
121 investigate whether Aqp8bb is trafficked to the mitochondria of activated spermatozoa
122 of FW teleosts as observed in the marine gilthead seabream (26), we first confirmed that
123 the Aqp8bb orthologs of Atlantic salmon and zebrafish are expressed in intratesticular
124 and ejaculated spermatozoa (*SI Appendix*, Figs. S1 and S2). Immunofluorescence
125 microscopy of sperm maintained in the corresponding non-activating medium (NAM),
126 previously loaded with the mitochondrion-specific vital dye MitoTracker Red CMXRos
127 (MTR), and using species-specific affinity-purified Aqp8bb antibodies, showed that the
128 seabream Aqp8bb peroxiporin was distributed in the midpiece region and anterior part
129 of the flagellum in immotile sperm, whereas in salmon and zebrafish Aqp8bb was
130 mostly located in more discrete areas surrounding the spermatozoon head (Fig. 1A-C).
131 Upon SW- (seabream) or FW- (salmon and zebrafish) activation of sperm motility,
132 Aqp8bb was rapidly accumulated in the mitochondria of each species (Fig. 1 A-C).
133 Quantification of immotile and motile spermatozoa showing co-localization of Aqp8bb
134 and MTR signals indicated that >75% of activated spermatozoa from each species
135 showed Aqp8bb mitochondrial accumulation (Fig. 1D-F), revealing that the peroxiporin
136 trafficking mechanism during sperm motility is a conserved trait in teleosts.

137

138 **Signaling pathways involved in Aqp8bb intracellular trafficking in SW**
139 **spermatozoa.** To uncover the signaling pathways involved in the Aqp8bb trafficking
140 mechanism of seabream spermatozoa, we used a battery of protein kinase inhibitors and
141 activators (Fig. 2, and *SI Appendix*, Table S1). Immunofluorescence microscopy and
142 immunoblotting data showed that the transit of Aqp8bb to the SW-activated sperm
143 mitochondrion was strongly inhibited in a dose-dependent manner by the JNK inhibitor
144 SP600125 with respect to spermatozoa treated with dimethyl sulfoxide (DMSO) vehicle
145 (control), whereas CHIR99021 and BIM-II, typical blockers of GSK3 and PKC,
146 respectively, also reduced Aqp8bb transport but were less effective (Fig. 2 A and B). By
147 contrast, inhibitors of p38 mitogen-activated protein kinase (p38 MAPK) and protein
148 kinase A (PKA), such as SB202190 and BIRB796, and H-89, respectively, showed no
149 effect (Fig. 2 A and B). We further tested the effect of inhibitors of several JNK
150 upstream regulators, including the MAPKKs MAP3K7/TAK1, germinal center
151 kinases (GCKs), apoptosis signal-regulating kinase 1 (ASK1) and mitogen-activated
152 protein kinase kinases (MKKs) (34), on Aqp8bb trafficking, using the compounds
153 NG25, GNF-7, NQDI-1 and PD98059. The data indicated that only ASK1 and MKKs
154 inhibitors can reduce Aqp8bb mitochondrial accumulation in a dose-dependent manner
155 (Fig. 2 A and B), suggesting that a canonical ASK1-MKK-JNK cascade, as well as a
156 PKC and GSK3 signaling pathways, regulate Aqp8bb trafficking in activated seabream
157 spermatozoa.

158 Immunoblotting experiments confirmed the expression of ASK1, MKK4, JNK
159 and GSK3 α/β kinases in immotile seabream spermatozoa (*SI Appendix*, Fig. S3A). Upon
160 the hyperosmotic shock in SW, the phosphorylation of MKK4^{T261}, JNK^{T183/Y185} and
161 GSK3 α/β ^{Y279/216} increased, whereas the inhibitory phosphorylation of ASK1^{S966} and
162 GSK3 α ^{S21} decreased, suggesting that the catalytic activities of all of these kinases are
163 activated (35-37). The inhibitory phosphorylation of GSK3 β ^{S9} seems not to be involved
164 during seabream sperm activation, since phosphorylated GSK3 β ^{S9} was detected in testis

165 extracts but not in spermatozoa (*SI Appendix*, Fig. S3B). Phosphorylation of
166 JNK^{T183/Y185} in SW-activated sperm was not affected by inhibitors of JNK, p38 MAPK,
167 PKA or GSK3 kinetic activity (Fig. 2C). However, JNK^{T183/Y185} phosphorylation was
168 reduced by PKC inhibition, although not completely, whereas that of Gsk3 α/β ^{Y279/216}
169 was partially decreased by both PKC and JNK blockage (Fig. 2C). Upon SW activation,
170 the respective inhibition of the JNK upstream kinases ASK1 and MKK4 decreased
171 MKK4^{T261}, JNK^{T183/Y185} and GSK3 α/β ^{Y279/216} phosphorylation (Fig. 2C), which is in
172 accordance with the known role of ASK1 phosphorylating MKK4 (34) and the ability of
173 PD98059 to prevent MKKs activation (38). Together, these data suggest that the ASK1-
174 MKK4-JNK cascade can partially activate GSK3, and that PKC activity is required for
175 full JNK and GSK3 activation. This combination can explain the somewhat lower
176 potency of PKC inhibition to prevent Aqp8bb mitochondrial transport. However, the
177 strong reduction of Aqp8bb trafficking by JNK inhibition suggests an additional role of
178 JNK on channel trafficking that is not mediated by GSK3.

179 In order to assess the potential interaction of the JNK, PKC and GSK3 pathways
180 in the regulation of Aqp8bb mitochondrial transport, we investigated whether this
181 mechanism could be stimulated in immotile spermatozoa. For this, NAM maintained
182 sperm were treated with the JNK/p38 MAPK phosphorylation-inducer anisomycin
183 (ANS) and the PKC analog activator phorbol 12-myristate 13-acetate (PMA), as well as
184 with MK2206 and SH-5, which are AKT/PKB inhibitors that can indirectly activate
185 GSK3 (39, 40). The data show that all of these drugs stimulated Aqp8bb mitochondrial
186 trafficking, while treatment with the PKC inactive enantiomer 4 α -PMA had no effect
187 (Fig. 2 D and E, and *SI Appendix*, Fig. S4A). However, the percentage of spermatozoa
188 showing Aqp8bb localization in the mitochondrion after exposure to ANS was similar
189 to that observed in SW-activated sperm, whereas the other compounds only promoted
190 channel mitochondrial accumulation in approximately half of the cells (Fig. 2 D and E,
191 and *SI Appendix*, Fig. S4A). The stimulatory effect of ANS on Aqp8bb trafficking,
192 which occurs through JNK and not p38 MAPK (*SI Appendix*, Fig. S3 B and C), was
193 completely blocked by GSK3 inhibition, but only partially reduced by the PKC
194 inhibitors BIM-II and calphostin C (Fig. 2 D and E, and *SI Appendix*, Fig. S4A). This
195 suggests that PKC activation by JNK is necessary to drive Aqp8bb mitochondrial
196 transport, but that this mechanism can still be triggered to some extent by JNK
197 independently of PKC. The positive effects of PMA and MK2206 on Aqp8bb transport
198 were not additive and could be reduced by JNK and GSK3 inhibition (*SI Appendix*, Fig.
199 S4 D and E), suggesting that PKC and GSK3 activate the same mechanism for Aqp8bb
200 trafficking, with both kinases dependent on active JNK.

201 Activation of JNK and PKC by ANS and PMA treatments, respectively, in
202 immotile spermatozoa induced the phosphorylation of JNK^{T183/Y185} and
203 GSK3 α/β ^{Y279/216}, thus supporting that JNK and GSK3 can be activated via PKC, and
204 that activation of GSK3 by JNK occurs during Aqp8bb trafficking (Fig. 2F). By
205 contrast, MK2206 activated GSK3 but not JNK, indicating that GSK3 is downstream of
206 JNK (Fig. 2F). However, as noted earlier, active JNK was still necessary for MK2206-
207 induced Aqp8bb transport, thus supporting a role of JNK regulating mitochondrial
208 Aqp8bb transport independently of GSK3. The ANS-mediated JNK^{T183/Y185}
209 phosphorylation was not affected by PKC or GSK3 inhibition, while that of
210 GSK3 α/β ^{Y279/216} was moderately reduced by PKC inhibition but it was not affected by
211 the GSK3 blocker (Fig. 2F). Therefore, this also confirms that JNK can partially
212 activate GSK3 in the absence of PKC activation.

213 Taken together, our findings suggest that a cross-talk between the PKC and JNK
214 signaling pathways triggers the GSK3-mediated trafficking of the Aqp8bb poroiporin

215 to the inner mitochondrial membrane of the seabream spermatozoon (Fig. 2G).
216 Moreover, a direct additive action of JNK, which bypasses the GSK3 pathway, acts as a
217 multiplier for the rapid trafficking mechanism (Fig. 2G).

218

219 **GSK3 and JNK control Aqp8bb-mediated mitochondrial detoxification in**
220 **activated seabream spermatozoa.** Since JNK and GSK3 appear to be key regulators of
221 Aqp8bb trafficking, we investigated whether the pharmacological blockage of their
222 activities can impair Aqp8bb insertion into the spermatozoon inner mitochondrial
223 membrane and hamper H₂O₂ efflux. An Aqp8bb immunoblot of inner membrane
224 mitochondrial extracts from SW-activated spermatozoa confirmed that the amount of
225 mitochondrial Aqp8bb was lower in sperm treated with the JNK and GSK3 inhibitors
226 compared to controls (Fig. 3A). The low mitochondrial abundance of Aqp8bb in these
227 groups was associated with a reduced ability of mitochondria to transport H₂O₂ as
228 measured with the ROS-sensitive, cell permeable fluorescent dye 5-(and -6)-
229 chloromethyl-2',7'-dichlorodihydrofluorescein diacetate, acetyl ester (CM-H₂DCFDA)
230 (Fig. 3B). As a consequence, a higher accumulation of H₂O₂ in the spermatozoa exposed
231 to the JNK and GSK3 inhibitors with respect to controls was observed during activation
232 (Fig. 3C). The increased intracellular ROS was harmful to sperm function since time-
233 course monitoring of sperm motion kinetics using computer-assisted sperm analysis
234 (CASA) for up to 180 s revealed that both inhibitors reduced the percentage of motility
235 and progressivity of the spermatozoa, as well as their curvilinear velocity (VCL), with
236 respect to sperm treated with DMSO alone (Fig. 3D). However, the three sperm motion
237 parameters measured within the first 30 s post-activation were more diminished when
238 the JNK pathway is blocked (17 ± 1% and 35 ± 5% inhibition with the GSK3 and JNK
239 blockers, respectively, with respect to the controls; *n* = 9, *P* = 0.003, Student's *t*-test).
240 The addition of the mitochondria-targeted antioxidant Mito-TEMPO recovered sperm
241 motion kinetics within 60-70 s, except the reduction in the percentage of motile
242 spermatozoa induced by GSK inhibition (Fig. 3E). This suggests that GSK3 likely plays
243 other roles to maintain sperm motility in addition to mitochondrial Aqp8bb trafficking.
244 These observations are thus consistent with a role of the JNK and GSK3 signaling
245 pathways regulating Aqp8bb mitochondrial detoxification and the kinematic properties
246 of the spermatozoa.

247

248 **Intracellular Ca²⁺ and ROS trigger seabream Aqp8bb mitochondrial transport.**
249 We previously demonstrated that prevention of the intracellular Ca²⁺ surge that
250 normally occurs in seabream sperm upon SW activation partially inhibits mitochondrial
251 Aqp8bb trafficking (41), and that the SW-induced hyperosmotic shock increases ROS
252 levels in the spermatozoa (26). Since it is known that the ASK1-MAPK signaling
253 pathway can be activated by cellular oxidative stress (42), we hypothesize that elevated
254 intracellular concentrations of Ca²⁺ ([Ca²⁺]_i) and ROS linked to the hyperosmotic shock
255 in SW are the upstream signals in seabream spermatozoa triggering JNK and GSK3
256 activation and Aqp8bb intracellular trafficking.

257 To investigate this hypothesis, we first determined the contribution of Ca²⁺-
258 activated signaling pathways in the regulation of Aqp8bb mitochondrial transport by
259 treating immotile sperm with 3 mM Ca²⁺ in the presence of 10 μM of the Ca²⁺
260 ionophore A23187, which generates similar levels of [Ca²⁺]_i to those determined in SW-
261 activated sperm (Fig. 4A). Under these conditions, Aqp8bb transport to the
262 mitochondria was enhanced, but interestingly, the percentage of spermatozoa showing
263 mitochondrial localization of the channel was approximately half of that observed in
264 SW-activated sperm (Fig. 4B). Ca²⁺-triggered Aqp8bb trafficking was not affected by

265 inhibitors of ASK1 and MKK, whereas it was reduced to control levels by blockers of
266 PKC, JNK and GSK3 (Fig. 4C, and *SI Appendix*, Fig. S5). After Ca^{2+} treatment, the
267 inhibitory phosphorylation of ASK1^{S966} did not change, and MKK4 was not activated,
268 while phosphorylation of JNK^{T183/Y185} and GSK3 α/β ^{Y279/216} was enhanced (Fig. 4D).
269 The activation of JNK and GSK3 was reduced by PKC inhibition, while the blockage of
270 JNK only partially diminished GSK3 activation (Fig. 4D). These data suggest that a
271 $[\text{Ca}^{2+}]_i$ surge alone can partially trigger JNK- and GSK3-mediated Aqp8bb
272 mitochondrial transport through PKC activation of JNK and GSK3, and thus
273 independently of the ASK1-MKK4 signaling pathway.

274 To examine the effect of oxidative stress on Aqp8bb intracellular trafficking in
275 spermatozoa, independently of the Ca^{2+} signal, we followed two different approaches:
276 the generation of ROS in immotile sperm by exposure to the xanthine-xanthine oxidase
277 (X-XO) system (43), and the treatment of SW-activated sperm with the Ca^{2+} chelator
278 1,2-bis(2-aminophenoxy)ethane-N,N,N',N'-tetraacetic acid (BAPTA) in the presence or
279 absence of diphenyleneiodonium (DPI), a compound that limits ROS production by
280 inhibiting membrane-bound NADPH oxidases (NOXes) and other flavoproteins (44).
281 External treatment of non-activated sperm with X-XO produced an increment of ROS in
282 a dose-response manner; the highest X-XO dose generating similar ROS levels to those
283 measured in SW-activated sperm (Fig. 5 A and D). Upon SW activation, treatment with
284 BAPTA abolished the $[\text{Ca}^{2+}]_i$ surge in a dose-dependent manner, which completely
285 inhibited motility (*SI Appendix*, Fig. S6A), while ROS accumulation in the spermatozoa
286 was not affected (Fig. 5 B and D). Conversely, exposure of activated sperm to DPI
287 decreased ROS levels but did not affect the increase of $[\text{Ca}^{2+}]_i$ (Fig. 5 C and D).
288 Interestingly, as previously observed in Ca^{2+} -treated immotile sperm, treatment of
289 immotile spermatozoa with the highest dose of X-XO stimulated Aqp8bb mitochondrial
290 trafficking in approximately half of the spermatozoa with respect to SW-activated
291 sperm exposed to DMSO alone (*SI Appendix*, Fig. S6B). The same result was observed
292 in sperm activated in SW containing BAPTA (*SI Appendix*, Fig. S6C).

293 In both ROS- and SW+BAPTA-treated spermatozoa, Aqp8bb mitochondrial
294 accumulation was completely inhibited by blockers of ASK1, MKK, JNK and GSK3,
295 whereas inhibition of PKC only partially decreased Aqp8bb transport (Fig. 5E, and *SI*
296 *Appendix*, Fig. S6 B-D). The ROS generated in immotile and SW spermatozoa activated
297 ASK1 by dephosphorylation of the inhibitory ASK1^{S966} site, which was not affected
298 by any of the downstream kinase inhibitors, while it enhanced the phosphorylation of
299 MKK4^{T261}, JNK^{T183/Y185} and GSK3 α/β ^{Y279/216} (Fig. 5F, and *SI Appendix*, Fig. S6E).
300 Activation of MKK4 was reduced to control levels by inhibitors of ASK1 and MKK,
301 but not by inhibition of downstream kinases, whereas ROS-induced JNK and GSK3
302 activation was completely blocked by ASK1 and MKK inhibitors, and only partially
303 prevented by PKC inhibition (Fig. 5F, and *SI Appendix*, Fig. S6E). However, JNK
304 inhibition strongly reduced ROS-mediated GSK3 activation (Fig. 5F, and *SI Appendix*,
305 Fig. S6E), which indicates that the ROS-triggered ASK1-MKK4-JNK pathway can
306 activate GSK3 independently of PKC. The data however also suggest that ROS-induced
307 PKC activity may be a positive regulator of JNK, as previously observed after Ca^{2+}
308 treatment alone, but that in this case this mechanism requires previous activation of JNK
309 by the canonical upstream kinase MKK4.

310 Consistent with this model, when either the $[\text{Ca}^{2+}]_i$ or ROS increments in SW-
311 activated sperm were completely abolished by BAPTA and DPI, respectively, the
312 percentage of spermatozoa showing mitochondrial localization was similar to that
313 elicited by ROS treatment of immotile spermatozoa, and was approximately half of that
314 observed in SW-activated sperm (Fig. 5 G and H). However, when both inhibitors were

315 present upon SW activation, Aqp8bb mitochondrial accumulation was strongly reduced
316 to the level observed in immotile spermatozoa (Fig. 5 G and H). Kinase phosphorylation
317 analysis showed that while ASK1 activation in SW-activated spermatozoa was not
318 affected by BAPTA treatment, DPI reduced both ASK1 and MKK4 activation (Fig. 5I).
319 In contrast, each of the BAPTA and DPI treatments only partially prevented JNK and
320 GSK3 activation (Fig. 5I). In the presence of BAPTA plus DPI, the activation state of
321 ASK1 and MKK4 did not change with respect to that observed in the presence of DPI
322 alone, whereas the activation of JNK and GSK3 was strongly diminished (Fig. 5I).

323 Taken together, these findings suggest that the intracellular Ca²⁺ and ROS signals
324 occurring in SW-activated seabream spermatozoa respectively trigger alternative and
325 additive PKC and ASK1-MAPK pathways, which cross-talk to activate JNK and GSK3
326 and direct Aqp8bb mitochondrial insertion.

327

328 **JNK and GSK3 can phosphorylate seabream Aqp8bb *in vitro*.** *In silico* analysis of
329 the seabream Aqp8bb amino acid sequence revealed the presence of three Ser residues
330 (Ser¹⁶, Ser¹⁹ and Ser²⁰) and one Thr (Thr²⁴) residue in the N-terminus of the channel as
331 potential phosphorylation recognition sites for GSK3 and proline-directed kinase (such
332 as p38 MAPK and JNK), respectively (Fig. 6A). An additional Ser residue (Ser⁹¹)
333 showing a low score for GSK3 and proline-directed kinase phosphorylation was also
334 identified in the first cytoplasmic loop (Fig. 6A). To experimentally assess whether
335 GSK3 and JNK can phosphorylate seabream Aqp8bb, we employed *in vitro*
336 phosphorylation assays using mouse recombinant JNK1 (rJNK1) and human
337 recombinant GSK3β (rGSK3). In these experiments, Flag-tagged Aqp8bb (Aqp8bb-
338 Flag) transiently expressed in embryonic kidney cells 293T (HEK293T) was
339 immunoprecipitated using the seabream Aqp8bb specific antibody and incubated with
340 rJNK1 or rGSK3β in the presence or absence of ATP. Immunoblotting of
341 immunoprecipitated Aqp8bb-Flag using phosphorylated Ser and Thr specific antibodies
342 confirmed the ATP-dependent specific phosphorylation of Aqp8bb Ser and Thr residues
343 by rJNK1, and only of Ser residues by rGSK3β (Fig. 6B). To determine which specific
344 channel residues are phosphorylated by the kinases, the same assays were carried out
345 using wild-type Aqp8bb-Flag (Aqp8bb-Flag-WT) or Aqp8bb-Flag constructs in which
346 all Ser and Thr residues in the N-terminus, as well as Ser⁹¹, were independently mutated
347 into Ala. The results showed that Aqp8bb-Flag-T24A and -S91A prevented rJNK1 Thr
348 and Ser phosphorylation, respectively, whereas Aqp8bb-Flag-S16A abolished Ser
349 phosphorylation by rGSK3β (Fig. 6C). These data therefore indicate that Thr²⁴ and Ser⁹¹
350 are the residues phosphorylated by rJNK1, while only Ser¹⁶ is the target site for
351 rGSK3β.

352 The majority of GSK3 substrates require pre-phosphorylation at a residue 4 or 5
353 amino acids C-terminal to the GSK3 target site for full catalytic activity, a phenomenon
354 referred to as ‘priming’ (45). The seabream Aqp8bb shows two such potential priming
355 sites, Ser¹⁹ and Ser²⁰, located 3 and 4 residues C-terminal to the Ser¹⁶ GSK3
356 phosphorylation site (Fig. 6A). In addition, Thr²⁴ could also play a role since some
357 substrates of GSK3 show a priming site much further from the target site (45). To
358 investigate whether a priming mechanism regulates rGSK3β-mediated Aqp8bb
359 phosphorylation at Ser¹⁶ we first established by immunoblotting the lowest amount of
360 rGSK3β to yield detectable levels of Ser phosphorylation in Aqp8bb (*SI Appendix*, Fig.
361 S7), and subsequently test if Aqp8bb-Flag-S19D, -S20D and -T24D mutants, which
362 mimic a phosphorylated state, increase rGSK3β-mediated channel phosphorylation. The
363 results show that Ser¹⁶ phosphorylation of Aqp8bb-Flag by rGSK3β was increased by
364 ~27 times in Aqp8bb-Flag-S19D and -S20D mutants with respect to the wild-type,

365 whereas the Aqp8bb-Flag-T24D was phosphorylated at Ser¹⁶ ~12 times more efficiently
366 (Fig. 6D). These findings therefore suggest that Aqp8bb phosphorylation of Ser¹⁹, Ser²⁰,
367 and to a lesser extent Thr²⁴, can prime the channel N-terminus for Ser¹⁶ phosphorylation
368 by GSK3 (Fig. 6E).

369

370 **GSK3 and JNK phosphorylation of Ser¹⁶ and Thr²⁴, respectively, in seabream**
371 **Aqp8bb regulate channel trafficking.** Transcriptional and translational activity in
372 ejaculated sperm is very low or completely absent (46). Therefore, in order to
373 investigate the molecular basis of Aqp8bb mitochondrial trafficking, we examined
374 whether the signaling pathways controlling this mechanism in spermatozoa can be
375 reproduced in cultured mammalian cells. For these tests, we selected the human
376 hepatocarcinoma-derived cell line HepG2 in which the AQP8 ortholog is expressed in
377 the inner mitochondrial membrane (47). The results of these experiments showed that
378 the same Ca²⁺-activated PKC-GSK3 and H₂O₂-activated JNK-GSK3 signaling cascades
379 controlling Aqp8bb mitochondrial transport in the seabream spermatozoon can be
380 replicated in HepG2 cells, except that in this case the cross-talk between PKC and JNK
381 does not occur (*SI Appendix*, Text S1).

382 Using the HepG2 cells as a surrogate system for functional analyses, we
383 investigated the role of Aqp8bb phosphorylation on mitochondrial channel trafficking.
384 To this end, we transfected cells with Aqp8bb-Flag-WT or single phosphomimetic
385 mutants at each Ser and Thr residue in the N-terminus of the channel (Aqp8bb-Flag-
386 T2D, -T15D, -S16D, -S19D, -S20D, -T24D), and at Ser⁹¹ (Aqp8bb-Flag-S91D), or with
387 a S16D/T24D double mutant, and subsequently determined mitochondrial targeting of
388 the encoded proteins by immunofluorescence microscopy. The data showed that
389 Aqp8bb-Flag-WT and the Aqp8bb-Flag-S91D mutant mainly remained in the cell
390 plasma membrane, whereas the Aqp8bb-Flag-T2D and -T15D channels were retained in
391 the cytoplasm (Fig. 7A, and *SI Appendix*, Fig. S9A). By contrast, the Aqp8bb-Flag-
392 S19D and -S20D mutants were partially targeted to the mitochondria, which appears to
393 be enhanced for the Aqp8bb-Flag-S16D, -T24D and S16D/T24D channel constructs
394 (Fig. 7A). Immunoblot analysis showed that the wild-type and mutant channels were
395 expressed at similar levels, and confirmed that each of the Aqp8bb-Flag-S16D and -
396 T24D mutants were targeted to the mitochondria, unlike the Aqp8bb-Flag-WT (Fig.
397 7B). The Aqp8bb-Flag-S19D and -S20D constructs also accumulated in the
398 mitochondria but to a lesser amount than the Aqp8bb-Flag-S16D and -T24D mutants
399 (Fig. 7B). However, the data also revealed that the Aqp8bb-Flag-S16D/T24D double
400 mutant was more concentrated in the mitochondria than each of the corresponding
401 single mutants (Fig. 7B), suggesting that phosphorylation of Ser¹⁶ and Thr²⁴ residues in
402 the channel are additive for activating mitochondrial transport.

403 To further investigate the role of Ser¹⁶ and Thr²⁴ phosphorylation driving Aqp8bb
404 mitochondrial trafficking, cells were transfected with Aqp8bb-Flag-WT or mutant
405 channels in which one or both Ser¹⁶ and Thr²⁴ were mutated into Cys or Ala,
406 respectively, and treated with 10 mM Ca²⁺ and 100 μM H₂O₂. Immunoblot analyses of
407 total protein extracts showed that the three Aqp8bb-Flag-S16C, -T24A and -S16C/T24A
408 mutants were equally expressed than the Aqp8bb-Flag-WT (*SI Appendix*, Fig. S9B).
409 However, mitochondrial trafficking in response to Ca²⁺ and H₂O₂ treatment was
410 similarly reduced in both Aqp8bb-Flag-S16C and -T24A constructs with respect to that
411 shown by the Aqp8bb-Flag-WT, whereas channel transport of the Aqp8bb-Flag-
412 S16C/T24A double mutant was almost completely abolished (Fig. 7C).
413 Immunoprecipitation followed by immunoblot analysis of phosphorylated Ser and Thr
414 showed that Aqp8bb-Flag-WT was phosphorylated at Ser and Thr residues in response

415 to Ca^{2+} and H_2O_2 uptake (Fig. 7C). However, only Ser or Thr phosphorylation was
416 reduced in the Aqp8bb-Flag-S16C and -T24A constructs, respectively, with respect to
417 that seen in the Aqp8bb-Flag-WT, while phosphorylation of both Ser and Thr residues
418 was decreased in the Aqp8bb-Flag-S16C/T24A double mutant (Fig. 7C). These data
419 therefore support that Ser¹⁶ and Thr²⁴ phosphorylation in the Aqp8bb N-terminus are
420 both necessary for maximum mitochondrial channel transport.

421 To determine whether GSK3 and JNK are respectively involved in Ser¹⁶ and Thr²⁴
422 phosphorylation of Aqp8bb, HepG2 cells were cotransfected with Aqp8bb-Flag-WT
423 and dominant-negative catalytically inactive forms of *Xenopus laevis* GSK3 β
424 (dnGSK3 β) (48) or human JNK1 (dnJNK1) (49), and exposed to external Ca^{+2} and
425 H_2O_2 . Both inhibitory constructs reduced the accumulation of Aqp8bb-Flag-WT in the
426 mitochondria in response to external Ca^{2+} and ROS (Fig. 7D), thus further supporting
427 the role of JNK and GSK3 in the Aqp8bb trafficking mechanism. However, while
428 dnGSK3 β expression decreased Ser phosphorylation of Aqp8bb-Flag-WT, but not Thr
429 phosphorylation, the dnJNK1 construct completely abolished Ser and Thr
430 phosphorylation of the channel (Fig. 7D). These findings suggest that JNK could
431 activate GSK3 for Aqp8bb Ser phosphorylation, in addition to its potential role
432 phosphorylating Thr²⁴ in the channel, as previously predicted to occur in sperm cells. To
433 corroborate this hypothesis, activation of GSK3 was evaluated in HepG2 cells
434 expressing Aqp8bb-Flag-WT and dnJNK1 and treated with Ca^{2+} and H_2O_2 . The data
435 confirmed that phosphorylation of GSK3 α/β ^{Y279/216} was reduced in the presence of
436 catalytically inactive JNK1, whereas that of GSK3 α ^{S21}, but not of GSK3 β ^{S9}, was
437 increased (Fig. 7E). These results therefore suggest that mitochondrial trafficking of
438 seabream Aqp8bb is regulated by Ser¹⁶ phosphorylation by JNK- and PKC-activated
439 GSK3, as well as by JNK-mediated Thr²⁴ phosphorylation of the channel.

440

441 **Aqp8bb mitochondrial transport in FW spermatozoa is controlled by PKC or**
442 **GSK3 phosphorylation of an N-terminal Ser residue.** To examine whether the same
443 signaling pathways regulating seabream Aqp8bb mitochondrial transport are present in
444 FW spermatozoa, we initially assessed the effect of PKC, JNK and GSK3 inhibitors
445 (BIM-II, SP600125 and CHIR99021, respectively) on Aqp8bb trafficking in Atlantic
446 salmon and zebrafish spermatozoa upon FW activation. In contrast to the seabream, the
447 results showed that JNK inhibition did not affect mitochondrial channel transport in
448 salmon and zebrafish sperm, indicating that the JNK signaling pathway is not involved
449 in this mechanism (Fig. 8A). In contrast, both PKC and GSK3 inhibitors reduced the
450 percentage of salmon spermatozoa showing Aqp8bb mitochondrial localization in a
451 dose-response manner, whereas only the blockage of PKC elicited the same effect in
452 zebrafish (Fig. 8A). These observations suggest a role of PKC and GSK3, and of PKC
453 only, in the control of Aqp8bb transport in salmon and zebrafish spermatozoa,
454 respectively.

455 To confirm that PKC is the signaling kinase controlling Aqp8bb-mediated
456 mitochondrial detoxification in zebrafish spermatozoa, the levels of ROS in immotile
457 and FW-activated sperm in the presence or absence of the PKC inhibitor BIM-II were
458 determined. The results showed that the hypoosmotic shock in FW does not increase
459 ROS levels in zebrafish sperm, however when the transport of Aqp8bb to the
460 mitochondria was impaired by PKC inhibition, ROS levels were increased (Fig. 8B).
461 This reveals that an osmotic shock-induced ROS-MAPK-JNK signaling pathway
462 controlling Aqp8bb trafficking is absent in zebrafish spermatozoa. As observed for
463 seabream sperm, high levels of intracellular ROS induced by PKC inhibition also
464 reduced the percentage of motility and progressivity and the VCL of zebrafish

465 spermatozoa (Fig. 8C). However, in this case Mito-TEMPO treatment only partially
466 recovered the kinematic properties (Fig. 8D), suggesting that PKC plays an additional
467 role for sperm motility and velocity maintenance in zebrafish that is unrelated to the
468 mitochondrial peroxiporin transport mechanism.

469 Comparison of the deduced amino acid sequences of the Aqp8bb N-terminus from
470 seabream, salmon and zebrafish revealed a Ser residue in position 14 or 16 in all three
471 species, whereas the JNK Thr²⁴ phosphorylation site from seabream Aqp8bb was
472 missing in the two FW spawning teleosts. *In silico* analysis revealed that Ser¹⁴ from
473 salmon Aqp8bb is a putative phosphorylation site for GSK3 as is Ser¹⁶ from seabream
474 Aqp8bb, including a potential priming site at Ser¹⁸, whereas Ser¹⁶ in zebrafish Aqp8bb
475 is a presumed residue for PKC phosphorylation (Fig. 8E). To confirm that these target
476 sites in salmon and zebrafish Aqp8bb are functional, *in vitro* phosphorylation assays
477 were performed in HEK293 cells as previously described. In this case, we tested
478 rGSK3 β and recombinant *X. laevis* PKC α (rPKC α) on Aqp8bb-Flag-WT and mutant
479 channels, in which Aqp8bb Ser¹⁴ (salmon) or Ser¹⁶ (zebrafish) were replaced by Ala.
480 Immunoblot results showed that salmon Aqp8bb-Flag-WT was equally phosphorylated
481 by rPKC α and rGSK3 β at Ser residues, whereas rGSK3 β was no longer able to
482 phosphorylate Ser residues in the Aqp8bb-Flag-S14A mutant, and only Ser
483 phosphorylation by rPKC α was detected (Fig. 8F). Similarly, zebrafish Aqp8bb-Flag-
484 WT was Ser phosphorylated by rPKC α and rGSK3 β , but the Aqp8bb-Flag-S16A mutant
485 could only be phosphorylated by rGSK3 β (Fig. 8F). These data indicate that salmon
486 Aqp8bb Ser¹⁴ and zebrafish Aqp8bb Ser¹⁶ are respectively the target residues of
487 rGSK3 β , and rPKC α . However, both salmon and zebrafish channels contain other
488 residues that are phosphorylated by rPKC α and rGSK3 β , respectively.

489 Finally, we transiently expressed salmon and zebrafish Aqp8bb-Flag-WT in
490 HepG2 cells and determined the effect of external Ca²⁺ and/or H₂O₂ on mitochondrial
491 channel localization. In contrast to seabream, Aqp8bb immunostaining of MTR loaded
492 cells, as well as immunoblotting of mitochondrial extracts, showed that only Ca²⁺ was
493 able to traffic both salmon and zebrafish Aqp8bb-Flag-WT to the mitochondria (*SI*
494 *Appendix*, Fig. S10 A and B). Since Ser¹⁴ and Ser¹⁶ from salmon and zebrafish Aqp8bb
495 are respectively the target sites of Ca²⁺-activated GSK3 and PKC, we investigated
496 whether phosphomimetic mutations at these sites could induce mitochondrial targeting
497 of the channels. For salmon Aqp8bb, we also tested Ser²⁰ in case this residue could play
498 a role as a priming site for GSK3 phosphorylation. All constructs were expressed at
499 similar levels in HepG2 cells (*SI Appendix*, Fig. S10 C and D), but immunostaining and
500 immunoblotting data indicated that only the salmon Aqp8bb-Flag-S14D and zebrafish
501 Aqp8bb-Flag-S16D mutants were constitutively targeted to the mitochondria (Fig. 8G-
502 J, *SI Appendix*, Fig. S10C). Taken together, these data suggest that Ca²⁺-activated PKC
503 or the PKC/GSK3 cascade are the effective pathways phosphorylating Ser¹⁶ or Ser¹⁴ in
504 the N-terminus of zebrafish and salmon Aqp8bb, respectively, which traffic the
505 peroxiporin to the mitochondria.

507 Discussion

508
509 The present work reveals new insight into the evolution of molecular mechanisms
510 regulating spermatozoan kinematic properties in an infraclass of vertebrates that display
511 intense levels of sperm competition. The data show that the rapid mitochondrial
512 trafficking of an Aqp8bb peroxiporin first discovered in a marine teleost (26), is
513 consistently regulated through N-terminal phosphorylation in FW and SW teleosts.
514 Such channel regulation thus represents a conserved mechanism of mitochondrial ROS

515 detoxification for the maintenance of ATP production and improved spermatozoon
516 performance.

517 The model arising from the data (Fig. 9) suggest that the signal transduction
518 pathways regulating Aqp8bb trafficking in teleost spermatozoa evolved increasing
519 levels of sophistication and cross-talk between the pathways through the inclusion of
520 alternative kinase cascade modules. Thus, in older lineages of FW teleost in which
521 spermatozoon motility is activated through hypoosmotic shock, a more direct Ca^{2+} -
522 PKC-mediated pathway phosphorylating the Aqp8bb N-terminus suffices (Fig. 9).
523 However, in the protacanthopterygian FW salmonids, in which the importance of sperm
524 velocity under sperm competition is well known (50), a PKC-regulated GSK3 cascade
525 is added and the channel is only phosphorylated by GSK3 to induce its trafficking (Fig.
526 9). The addition of the extra GSK3 regulatory layer may act as a multiplier if the
527 expression levels of this kinase significantly exceed those of PKC, a facet that could
528 explain the higher sperm velocities of sedentary parasitic males compared to
529 anadromous “bourgeois” males (51). In contrast to the FW species, we find that marine
530 spermatozoa have recruited an additional ROS-triggered JNK pathway to cope with the
531 elevated hypertonic stress (Fig. 9). In this case, JNK directly activates GSK3, but also
532 crosstalks with Ca^{2+} - and ROS-activated PKC to trigger Aqp8bb N-terminal
533 phosphorylation by GSK3, thus creating a multiplier pathway for the regulation of the
534 peroxiporin trafficking. In addition, JNK bypasses the GSK3 pathway to directly
535 phosphorylate the channel in a different N-terminal residue, further enhancing the
536 peroxiporin trafficking.

537 The conserved action of PKC in each of the pathways regulating Aqp8bb
538 trafficking in FW and SW spermatozoa reveals how the multiplier mechanism evolved.
539 In SW-activated spermatozoa, both Ca^{2+} and ROS induce PKC activity, with ROS also
540 inducing JNK activity through the ASK1-MKK4 cascade to further enhance PKC
541 catalysis, which together with the direct activation of GSK3 by JNK, multiplies the
542 action of GSK3 to phosphorylate Aqp8bb (Fig. 9). The importance of this stress-
543 induced multiplier pathway is clearly evident on the spermatozoon kinematic properties,
544 where JNK inhibition more rapidly suppresses the degree of motility, progressivity and
545 velocity of spermatozoa compared to GSK3 inhibition. Consequently, it seems likely
546 that positive selection of the JNK pathway with efficient catalytic kinetics would be
547 advantageous in the sperm competition of SW species, while those of the PKC and
548 GSK3 pathways would be favourable for FW species.

549 Interestingly, with the exception of the cross-talk between JNK and PKC to
550 activate GSK3, we were able to replicate the signalling pathways regulating
551 mitochondrial Aqp8bb trafficking in piscine spermatozoa in human cells. This finding
552 suggests that these signal transduction pathways are ancient and were likely present in
553 the last common ancestor of mammals and fishes (>435 million years ago) (52).
554 However, although ROS transport is involved in normal human spermatozoa
555 functioning, and AQP8 has been observed in the midpiece and likely in the
556 mitochondria (53-54), it is not yet clear whether AQP8 functions as a mitochondrial
557 peroxiporin in mammalian sperm. If indeed AQP8 is an orthologous mitochondrial
558 peroxiporin contributing to the kinematic properties of vertebrate spermatozoa, it will be
559 revealing to identify whether the same JNK and GSK3 pathways are involved in AQP8
560 trafficking mechanisms.

561 In mammals, the Ser/Thr kinase GSK3 is encoded by two paralogous genes
562 (*GSK3 α* and *GSK3 β*), the activities of which are regulated by post-translational
563 Ser²¹/Ser⁹ and Tyr²⁷⁹/Tyr²¹⁶ phosphorylation (37). It is now well recognized that the
564 *GSK3 α* enzyme plays an important role in the acquisition of sperm motility and

565 acrosomal reaction in mammals (55-57). The inhibitory GSK3 α ^{S21} phosphorylation is
566 high during the epididymal sperm maturation stage, but subsequently decreases to
567 activate the kinase activity during the hyperactivation phase in the female oviduct (58-
568 61). This latter mammalian hyperactivation mechanism is reminiscent of the activation
569 of motility in marine fish spermatozoa (31), which is also associated with the
570 dephosphorylation of GSK3 α ^{S21} as demonstrated here in the seabream. In teleosts,
571 however, the role of GSK3 on spermatozoon function has remained largely unknown,
572 although a recent study in zebrafish has shown that the knockout of miR-34a, which
573 normally downregulates GSK3, enhances sperm motility and the fertilization rates (62).
574 Since we show that GSK3 is not involved in the peroxiporin trafficking mechanism in
575 zebrafish spermatozoa, it seems likely that this kinase controls other elements of the
576 motility. Indeed, the inability of the antioxidant mito-TEMPO to rescue seabream
577 spermatozoa motility, when inhibited by the GSK3 blocker CHIR99021, supports the
578 notion that GSK3 plays additional motility activation roles unrelated to Aqp8bb
579 mitochondrial detoxification.

580 In contrast to GSK3, the role of the stress-activated JNK cascade for
581 spermatozoon motility in vertebrates is less well known. This pathway is involved in
582 both pro-apoptotic and anti-apoptotic mechanisms in response to various stimuli, such
583 as osmotic and oxidative stress (63). The data available for mammalian spermatozoa
584 suggest a role for JNK in cell survival under osmotic stress (64), as well as during
585 progesterone-induced hyperactivation (65). Such a role of JNK during osmotic stress is
586 consistent with the results of the present study showing the involvement of the JNK
587 signaling pathway controlling Aqp8bb-mediated mitochondrial detoxification in marine
588 spermatozoa. Interestingly, in the non-flagelated spermatozoa of the nematode
589 *Caenorhabditis elegans*, both Ca²⁺ and the MAPK cascade, which functions
590 downstream of, or parallel with, the Ca²⁺ signaling, are necessary for sperm activation
591 (66). This resembles the molecular scenario controlling Aqp8bb trafficking in seabream
592 spermatozoa. In addition, pharmacological activation of JNK/p38 MAPK is sufficient to
593 trigger sperm motility acquisition in *C. elegans* (66), while the same treatment of
594 immotile seabream sperm bypasses the requirement of the Ca²⁺ signal for the induction
595 of mitochondrial Aqp8bb transport. Therefore, although nematode and fish spermatozoa
596 are morphologically distinct, and their motility is regulated by different molecular
597 machineries, both types of spermatozoa appear to utilize conserved signaling pathways
598 for different purposes, to modulate sperm maturation in the case of the nematode, or to
599 insert a peroxiporin in the mitochondrion of the seabream spermatozoon as an anti-
600 apoptotic mechanism.

601 Our pharmacological studies in seabream sperm and HepG2 cells suggest a
602 complex cascade of kinase phosphorylation events, where PKC- and JNK-mediate
603 GSK3 activation by GSK3 α/β ^{Y279/216} phosphorylation, and PKC activates JNK and
604 viceversa. However, both PKC and JNK are Ser/Thr kinases, and in ejaculated
605 mammalian spermatozoa PKC inhibits, rather than activates, GSK3 activity by
606 GSK3 α ^{S21} inhibitory phosphorylation (67-69). In contrast, in colon cancer cells the
607 atypical PKC ζ isoform can rapidly and transiently activate GSK3 β activity through
608 Ser¹⁴⁷ phosphorylation, which is also required to maintain the constitutive basal activity
609 of GSK3 β (69). Although a PKC ζ ortholog is expressed in fish sperm (70), the role of
610 this specific kinase regulating GSK3 and Aqp8bb mitochondrial transport requires
611 further investigation. The PKC-mediated GSK3 α/β ^{Y279/216} phosphorylation occurring in
612 seabream sperm could also be an indirect mechanism, as it seems to occur during the
613 activation of GSK3 by JNK, or the activation of JNK by PKC. The latter would
614 resemble the Toll-like receptor 4-Transient receptor potential channel 1-PKC α signaling

615 pathway that is triggered as defense and proinflammatory response to bacterial infection
616 (71), in which PKC may phosphorylate Ser¹²⁹ in JNK augmenting its phosphorylation
617 by MKK4 (72). The JNK-mediated activation of GSK3 has been reported to take place
618 in a hepatocyte cell line through the MAP3K mixed-lineage kinase 3 in a positive
619 feedback mechanism (73). A similar indirect mechanism mediating the activation of
620 GSK3 by JNK might occur through stimulation of the proline-rich tyrosine kinase 2,
621 which is a Ca²⁺-activated tyrosine kinase in capacitated human sperm (74), or through
622 the Src-related tyrosine kinase Fyn (75).

623 The present study provides new evidence suggesting that piscine Aqp8bb is a
624 physiological substrate of PKC, GSK3 and JNK, which regulate channel trafficking.
625 This is supported by the demonstration that these kinases can phosphorylate the
626 different teleost Aqp8bb orthologs *in vitro*, and that mutations of the respective target
627 sites trigger or abolish mitochondrial channel transport. In the seabream model, it is also
628 supported by the observation that inhibition of GSK3 and JNK activity through the
629 expression of dominant-negative forms of the kinases in HepG2 cells specifically
630 reduces the phosphorylation of the target sites in the channel and impairs mitochondrial
631 trafficking. The phosphorylation of Aqp8bb by JNK at Thr²⁴ could play a role as a
632 priming mechanism for subsequent GSK3 phosphorylation since our *in vitro* data show
633 that mimicking a constitutive phosphorylated state of this site can enhance GSK3
634 phosphorylation of Ser¹⁶ in the channel. This would agree with the observation that
635 under cell stress JNK can phosphorylate antiapoptotic proteins priming them for
636 subsequent phosphorylation by GSK3 (45). However, we found that mutation of Thr²⁴
637 into Ala in seabream Aqp8bb to prevent its phosphorylation by JNK does not reduce
638 GSK3-mediated Ser phosphorylation of the channel in HepG2 cells during Ca²⁺ and
639 H₂O₂ stimulation. This therefore argues against a role of JNK as a priming kinase for
640 GSK3. Rather, our data indicate that GSK3 and JNK phosphorylation of Aqp8bb are
641 both required for maximum accumulation of the channel in the mitochondria.

642 In summary, this work presents a new mechanism of spermatozoon motility
643 regulation in animals. The data show that a conserved process of mitochondrial ROS
644 detoxification evolved in piscine spermatozoa to enhance their kinematic properties.
645 The detoxification process occurs through the rapid trafficking of an Aqp8bb
646 peroxiporin to the inner mitochondrial membrane to facilitate H₂O₂ efflux and the
647 continued production of ATP necessary for flagellar contractions. The signal
648 transduction cascades controlling the trafficking mechanism are rapidly activated in
649 ejaculated sperm through hydration in FW teleosts and dehydration in SW teleosts
650 leading to phosphorylation of Ser/Thr residues in the Aqp8bb N-terminus. The data
651 further reveal the evolution of an increasingly sophisticated hierarchy of kinases
652 activating the trafficking mechanism with more direct Ca²⁺-PKC or Ca²⁺-PKC-GSK3
653 induction pathways in ancient lineages of FW teleosts to a cross talk between the Ca²⁺-
654 PKC-GSK3 signaling mechanism and a ROS-activated JNK multiplier pathway in
655 modern lineages of marine teleosts. These findings uncover gene networks involved in
656 post-activated spermatozoon swimming performance and thus provide new insight into
657 the molecular controls that may form selective traits for post-copulatory sexual
658 selection.

659 **Materials and Methods**

661 Detailed information on fish species and sperm collection methods; reagents, antibodies and
662 DNA constructs; computational analysis of aquaporin structure; determination of sperm motion
663 kinetics using CASA; cell culture and transfection; aquaporin functional characterization in
664 *Xenopus* oocytes; isolation of mitochondria from sperm and cultured cells; dermination of ROS
665

666 and $[Ca^{2+}]_i$ levels in sperm and mitochondria; *in vitro* phosphorylation assays; Western blot
667 analysis; immunofluorescence microscopy; and statistical analysis are provided in *SI Appendix*,
668 *Materials and Methods*.

669
670 **Data Availability.** All study data are included in the article and *SI Appendix*.

671
672 **ACKNOWLEDGEMENTS.** We thank Prof. S. S. Madsen for providing Atlantic salmon
673 Aqp8aa, -8ab and -8bb specific antibodies. This work was supported by the Spanish Ministry of
674 Economy, Industry and Competitiveness (MINECO) (Grant no. AGL2016-76802-R to J.C) and
675 the Norwegian Research Council (Grant nos. 254872/E40 and 294768/E40 to R.N.F.). F.C. and
676 A.F. were supported, respectively, by a “Ramon y Cajal” contract (RYC-2015-17103) and a
677 predoctoral grant (BES-2014-068745) from Spanish MINECO.

678 **References**

- 680
681 1. M. J. Gage, P. Stockley, G. A. Parker, Effects of alternative male mating strategies on
682 characteristics of sperm production in the Atlantic salmon (*Salmo salar*): theoretical and
683 empirical investigations. *Phil. Trans. R. Soc. B* **350**, 391-399 (1995).
- 684 2. D. P. Froman, A. J. Feltmann, M. L. Rhoads, J. D. Kirby, Sperm mobility: A primary
685 determinant of fertility in the domestic fowl (*Gallus domesticus*). *Biol. Reprod.* **61**, 400-
686 405 (1999).
- 687 3. E. Kupriyanova, J. N. Havenhand, Variation in sperm swimming behaviour and its effect
688 on fertilization success in the serpulid polychaete *Galeolaria caespitosa*. *Invertebrate*
689 *Reprod. Dev.* **41**, 21-26 (2002).
- 690 4. T. Pizzari, G. A. Parker, “Sperm competition and sperm phenotype” in *Sperm Biology: an*
691 *Evolutionary Perspective*, T. R. Birkhead, D. J. Hosken, S. Pitnick, Eds. (Academic
692 Press, 2009), pp. 207-245.
- 693 5. E. Del Olmo, A. Bisbal, A. Maroto-Morales, O. García-Alvarez, M. Ramon *et al.*,
694 Fertility of cryopreserved ovine semen is determined by sperm velocity. *Anim. Reprod.*
695 *Sci.* **138**, 102-109 (2013).
- 696 6. R. K. Brown, S. A. Kaurova, V. K. Uteshev, N. V. Shishova, D. McGinnity, *et al.*, Sperm
697 motility of externally fertilizing fish and amphibians. *Theriogenology* **83**, 1-13 (2015).
- 698 7. A. M. Cancel, D. Lobdell, P. Mendola, S. D. Perreault, Objective evaluation of
699 hyperactivated motility in rat spermatozoa using computer-assisted sperm analysis. *Hum.*
700 *Reprod.* **15**, 1322-1328 (2000).
- 701 8. D. R. Levitan, Sperm velocity and longevity trade off each other and influence
702 fertilization in the sea urchin *Lytechinus variegatus*. *Proc. R. Soc. Lond B* **267**, 531-534
703 (2000).
- 704 9. T. R. Birkhead, F. M. Hunter, Mechanisms of sperm competition. *Trends Ecol. Evol.* **5**,
705 48-51 (1990).
- 706 10. M. J. Gage, C. P. Macfarlane, S. Yeates, R. G. Ward, J. B. Searle *et al.*, Spermatozoal
707 traits and sperm competition in Atlantic salmon: relative sperm velocity is the primary
708 determinant of fertilization success. *Curr. Biol.* **14**, 44-47 (2004).
- 709 11. S. Liljedal, G. Rudolfsen, I. Foldstad, Factors predicting male fertilization success in an
710 external fertilizer. *Behav. Ecol. Sociobiol.* **62**, 1805-1811 (2008).
- 711 12. J. L. Fitzpatrick, R. Montgomerie, J. K. Desjardins, K. A. Stiver, N. Kolm, *et al.*, Female
712 promiscuity promotes the evolution of faster sperm in cichlid fishes. *Proc. Natl. Acad.*
713 *Sci. U.S.A.* **106**, 1128-1132 (2009).
- 714 13. C. Gasparini, L. W. Simmons, M. Beveridge, J. P. Evans, Sperm swimming velocity
715 predicts competitive fertilization success in the green swordtail *Xiphophorus helleri*.
716 *PLoS One* **5**, e12146 (2010).
- 717 14. C. Boschetto, C. Gasparini, A. Pilastro, Sperm number and velocity affect sperm
718 competition success in the guppy (*Poecilia reticulata*). *Behav. Ecol. Sociobiol.* **65**, 813-
719 821 (2011).

- 720 15. M. Tourmente, M. Gomendio, E. R. Roldan, Sperm competition and the evolution of
721 sperm design in mammals. *BMC Evol. Biol.* **11**, 12 (2011).
- 722 16. G. A. Parker, Sperm competition and its evolutionary consequences in the insects. *Biol.*
723 *Rev.* **45**, 525-567 (1970).
- 724 17. G. A. Parker, T. Pizzar, Sperm competition and ejaculate economics. *Biol. Rev.* **85**, 897-
725 934 (2010).
- 726 18. P. Stockley, M. J. G. Gage, G. A. Parker, A. P. Møller, Sperm competition in fishes: The
727 evolution of testis size and ejaculate characteristics. *Am. Nat.* **149**, 933-954 (1997).
- 728 19. A. Civetta, J. M. Ranz, Genetic factors influencing sperm competition. *Front. Genetics*
729 **10**, 820 (2019).
- 730 20. R. C. Firman, L. W. Simmons, Sperm midpiece length predicts sperm swimming velocity
731 in house mice. *Biol. Lett.* **6**, 513-516 (2010).
- 732 21. T. V. Vladić, B. A. Afzelius, G. E. Bronnikov, Sperm quality as reflected through
733 morphology in salmon alternative life histories. *Biol. Reprod.* **66**, 98-105 (2002).
- 734 22. S. Lüpold, S. Calhim, S. Immler, T. R. Birkhead, Sperm morphology and sperm velocity
735 in passerine birds. *Proc. Biol. Sci.* **276**, 1175-1181 (2009).
- 736 23. E. de Lamirande, C. Gagnon, Reactive oxygen species and human spermatozoa. I. Effects
737 on the motility of intact spermatozoa and on sperm axonemes. *J. Androl.* **13**, 368-378
738 (1992).
- 739 24. E. de Lamirande, C. Gagnon, Reactive oxygen species and human spermatozoa. II.
740 Depletion of adenosine triphosphate plays an important role in the inhibition of sperm
741 motility. *J. Androl.* **13**, 379-386 (1992).
- 742 25. J. S. Armstrong, M. Rajasekaran, W. Chamulitrat, P. Gatti, W. J. Hellstrom, *et al.*,
743 Characterization of reactive oxygen species induced effects on human spermatozoa
744 movement and energy metabolism. *Free Radic. Biol. Med.* **26**, 869-880 (1999).
- 745 26. F. Chauvigné, M. Boj, R. N. Finn, J. Cerdà, Mitochondrial aquaporin-8-mediated
746 hydrogen peroxide transport is essential for teleost spermatozoon motility. *Sci. Rep.* **5**,
747 7789 (2015).
- 748 27. S. Sadeghi, J. Pertusa, K. L. Yaniz, J. Nuñez, C. Soler, *et al.*, Effect of different oxidative
749 stress degrees generated by hydrogen peroxide on motility and DNA fragmentation of
750 zebrafish (*Danio rerio*) spermatozoa. *Reprod. Domestic Anim.* **53**, 1498-1505 (2018).
- 751 28. L. Burnaugh, B. A. Ball, K. Sabeur, A. D. Thomas, S. A. Meyers, Osmotic stress
752 stimulates generation of superoxide anion by spermatozoa in horses. *Anim. Reprod. Sci.*
753 **117**, 249-260 (2010).
- 754 29. R. N. Finn, F. Chauvigné, J. B. Hlidberg, C. P. Cutler, J. Cerdà, The lineage-specific
755 evolution of aquaporin gene clusters facilitated tetrapod terrestrial adaptation. *PLoS One*
756 **9**, e113686 (2014).
- 757 30. E. Koren, J. Lukac, Mechanism of liquefaction of the human ejaculate I. Changes of the
758 ejaculate proteins. *J. Reprod. Fert.* **56**, 493-499 (1979).
- 759 31. J. Cosson, A. L. Groison, M. Suquet, C. Fauvel, C. Dreanno *et al.*, Marine fish
760 spermatozoa: racing ephemeral swimmers. *Reproduction* **136**, 277-294 (2008).
- 761 32. J. Cosson, "Fish sperm physiology: Structure, factors regulating motility, and motility
762 evaluation" in *Biological Research in Aquatic Science*, Y. Bozkurt, Ed. (IntechOpen,
763 2019), DOI: 10.5772/intechopen.85139.
- 764 33. G. N. Cherr, M. Morisawa, C. A. Vines, K. Yoshida, E. H. Smith, *et al.*, Two egg-derived
765 molecules in sperm motility initiation and fertilization in the Pacific herring (*Clupea*
766 *pallasi*). *Int. J. Dev. Biol.* **52**, 743-752 (2008).
- 767 34. R. J. Davis, Signal transduction by the JNK group of MAP kinases. *Cell* **103**, 239-252
768 (2000).
- 769 35. M. Yan, T. Dai, J. C. Deak, J. M. Kyriakis, L. I. Zon *et al.*, Activation of stress-activated
770 protein kinase by MEKK1 phosphorylation of its activator SEK1. *Nature* **372**, 798-800
771 (1994).
- 772 36. E. H. Goldman, L. Chen, H. Fu, Activation of apoptosis signal-regulating kinase 1 by
773 reactive oxygen species through dephosphorylation at serine 967 and 14-3-3 dissociation.
774 *J. Biol. Chem.* **279**, 10442-10449 (2004).

- 775 37. E. Beurel, S. F. Grieco, R. S. Jope, Glycogen synthase kinase-3 (GSK3): regulation,
776 actions, and diseases. *Pharmacol. Ther.* **148**, 114-131 (2015).
- 777 38. D. R. Alessi, A. Cuenda, P. Cohen, D. T. Dudley, A. R. Saltiel, PD 098059 is a specific
778 inhibitor of the activation of mitogen-activated protein kinase kinase *in vitro* and *in vivo*.
779 *J. Biol. Chem.* **270**, 27489-27494 (1995).
- 780 39. A. P. Kozikowski, H. Sun, J. Brognard, P. A. Dennis, Novel PI analogues selectively
781 block activation of the pro-survival serine/threonine kinase Akt. *J. Am. Chem. Soc.* **125**,
782 1144-1145 (2003).
- 783 40. S. F. Moore, M. T. van den Bosch, R. W. Hunter, K. Sakamoto, A. W. Poole *et al.*, Dual
784 regulation of glycogen synthase kinase 3 (GSK3) α/β by protein kinase C (PKC) α and Akt
785 promotes thrombin-mediated integrin α IIb β 3 activation and granule secretion in platelets.
786 *J. Biol. Chem.* **288**, 3918-3928 (2013).
- 787 41. M. Boj, F. Chauvigné, J. Cerdà, Coordinated action of aquaporins regulates sperm
788 motility in a marine teleost. *Biol. Reprod.* **93**, 40 (2015).
- 789 42. A. Matsuzawa, H. Ichijo, Redox control of cell fate by MAP kinase: physiological roles
790 of ASK1-MAP kinase pathway in stress signaling. *Biochim. Biophys. Acta* **1780**, 1325-
791 1336 (2008).
- 792 43. M. Hagedorn, M. McCarthy, V. L. Carter, S. A. Meyers, Oxidative stress in zebrafish
793 (*Danio rerio*) sperm. *PLoS One* **7**, e39397 (2012).
- 794 44. Y. Li, M. A. Trush, Diphenyleiodonium, an NAD(P)H oxidase inhibitor, also potently
795 inhibits mitochondrial reactive oxygen species production. *Biochem. Biophys. Res.*
796 *Commun.* **253**, 295-299 (1998).
- 797 45. C. Sutherland, What Are the bona fide GSK3 Substrates? *Int J Alzheimers Dis.* **2011**,
798 505-607 (2011).
- 799 46. X. Ren, X. Chen, Z. Wang, D. Wang, Is transcription in sperm stationary or dynamic? *J.*
800 *Reprod. Dev.* **63**, 439-443 (2017).
- 801 47. M. J. Marchissio, D. E. Francés, C. E. Carnovale, R. A. Marinelli, Mitochondrial
802 aquaporin-8 knockdown in human hepatoma HepG2 cells causes ROS-induced
803 mitochondrial depolarization and loss of viability. *Toxicol. Appl. Pharmacol.* **264**,
804 246-254 (2012).
- 805 48. V. F. Taelman, R. Dobrowolski, J. L. Plouhinec, L. C. Fuentealba, P. P. Vorwald *et al.*,
806 Wnt signaling requires sequestration of glycogen synthase kinase 3 inside multivesicular
807 endosomes. *Cell* **143**, 1136-1148 (2010).
- 808 49. B. Dérijard, M. Hibi, I. H. Wu, T. Barrett, B. Su *et al.*, JNK1: a protein kinase stimulated
809 by UV light and Ha-Ras that binds and phosphorylates the c-Jun activation domain. *Cell*
810 **76**, 1025-1037 (1994).
- 811 50. J. Beirão, T. B. Egeland, C. F. Purchase, J. T. Nordeide, Fish sperm competition in
812 hatcheries and between wild and hatchery origin fish in nature. *Theriogenology* **133**, 201-
813 209 (2019).
- 814 51. M. Taborsky, Sperm competition in fish: 'bourgeois' males and parasitic spawning.
815 *Trends Ecol. Evol.* **13**, 222-227 (2008).
- 816 52. S. Kumar, G. Stecher, M. Suleski, S. B. Hedges, TimeTree: A resource for timelines,
817 timetrees, and divergence times. *Mol. Biol. Evol.* **34**, 1812-1819 (2017).
- 818 53. U. Laforenza, G. Pellavio, A. L. Marchetti, C. Omes, F. Tadaró *et al.*, Aquaporin-
819 mediated water and hydrogen peroxide transport is involved in normal human
820 spermatozoa functioning. *Int. J. Mol. Sci.* **18**, 66 (2016).
- 821 54. G. Pellavio, F. Todaro, P. Alberizzi, C. Scotti, G. Gastaldi *et al.*, HPV infection affects
822 human sperm functionality by inhibition of Aquaporin-8. *Cells* **9**, 1241 (2020).
- 823 55. R. Bhattacharjee, S. Goswami, T. Dudiki, A. P. Popkie, C. J. Phiel *et al.*, Targeted
824 disruption of glycogen synthase kinase 3A (GSK3A) in mice affects sperm motility
825 resulting in male infertility. *Biol. Reprod.* **92**, 65 (2015).
- 826 56. A. T. Reid, A. L. Anderson, S. D. Roman, E. A. McLaughlin, A. McCluskey *et al.*,
827 Glycogen synthase kinase 3 regulates acrosomal exocytosis in mouse spermatozoa via
828 dynamin phosphorylation. *FASEB J.* **29**, 2872-2882 (2015).

- 829 57. S. Dey, A. Eisa, D. Kline, F. F. Wagner, S. Abeyirigunawardena *et al.*, Roles of
830 glycogen synthase kinase 3 alpha and calcineurin in regulating the ability of sperm to
831 fertilize eggs. *FASEB J.* **34**, 1247-1269 (2020).
- 832 58. S. Koch, S. P. Acebron, J. Herbst, G. Hatiboglu, C. Niehrs, Post-transcriptional Wnt
833 signaling governs epididymal sperm maturation. *Cell* **163**, 1225-1236 (2015).
- 834 59. M. J. Freitas, J. V. Silva, C. Brothag, B. Regadas-Correia, M. Fardilha *et al.*, Isoform-
835 specific GSK3A activity is negatively correlated with human sperm motility. *Mol. Hum.*
836 *Reprod.* **25**, 171-183 (2019).
- 837 60. S. Dey, C. Brothag, S. Vijayaraghavan, Signaling enzymes required for sperm maturation
838 and fertilization in mammals. *Front Cell Dev. Biol.* **7**, 341 (2019).
- 839 61. D. Martin-Hidalgo, R. Serrano, C. Zaragoza, L. J. Garcia-Marin, M. J. Bragado, Human
840 sperm phosphoproteome reveals differential phosphoprotein signatures that regulate
841 human sperm motility. *J. Proteomics* **215**, 103654 (2020).
- 842 62. W. Guo, B. Xie, S. Xiong, X. Liang, J. F. Gui, *et al.*, miR-34a regulates sperm motility in
843 zebrafish. *Int. J. Mol. Sci.* **18**, 2676 (2017).
- 844 63. J. Yue, J. M. López, Understanding MAPK signaling pathways in apoptosis. *Int. J. Mol.*
845 *Sci.* **21**, 2346 (2020).
- 846 64. B. M. García, A. M. Moran, L. G. Fernández, C. O. Ferrusola, Rodriguez AM, *et al.*, The
847 mitochondria of stallion spermatozoa are more sensitive than the plasmalemma to
848 osmotic-induced stress: role of c-Jun N-terminal kinase (JNK) pathway. *J. Androl.* **33**,
849 105-113 (2012).
- 850 65. V. Sagare-Patil, M. Galvankar, M. Satiya, B. Bhandari, S. K. Gupta *et al.*, Differential
851 concentration and time dependent effects of progesterone on kinase activity,
852 hyperactivation and acrosome reaction in human spermatozoa. *Int. J. Androl.* **35**, 633-644
853 (2012).
- 854 66. Z. Liu, B. Wang, R. He, Y. Zhao, L. Miao, Calcium signaling and the MAPK cascade are
855 required for sperm activation in *Caenorhabditis elegans*. *Biochim. Biophys Acta* **1843**,
856 299-308 (2014).
- 857 67. I. M. Aparicio, M. J. Bragado, M. C. Gil, M. Garcia-Herreros, L. Gonzalez-Fernandez *et*
858 *al.*, Porcine sperm motility is regulated by serine phosphorylation of the glycogen
859 synthase kinase-3alpha. *Reproduction* **134**, 435-444 (2007).
- 860 68. M. J. Bragado, I. M. Aparicio, M. C. Gil, L. J. Garcia-Marin, Protein kinases A and C and
861 phosphatidylinositol 3 kinase regulate glycogen synthase kinase-3A serine 21
862 phosphorylation in boar spermatozoa. *J. Cell Biochem.* **109**, 65-73 (2010).
- 863 69. N. Tejada-Muñoz, H. González-Aguilar, P. Santoyo-Ramos, M. C. Castañeda-Patlán, M.
864 Robles-Flores, Glycogen synthase kinase 3β is positively regulated by protein kinase Cζ-
865 mediated phosphorylation induced by Wnt agonists. *Mol. Cell Biol.* **36**, 731-741 (2016).
- 866 70. C. F. Huang, H. C. Chen, N. N. Chuang, C. M. Kuo, The zeta protein kinase C isoform
867 from the testis of the grey mullet *Mugil cephalus* with a specific reaction protein of M(r)
868 48,000 on oolemma. *Comp. Biochem. Physiol. C Pharmacol. Toxicol. Endocrinol.* **111**,
869 429-433 (1995).
- 870 71. X. Zhou, Y. Ye, Y. Sun, X. Li, W. Wang *et al.*, Transient receptor potential channel 1
871 deficiency impairs host defense and proinflammatory responses to bacterial infection by
872 regulating protein kinase Cα signaling. *Mol. Cell Biol.* **35**, 2729-2739 (2015).
- 873 72. P. López-Bergami, H. Habelhah, A. Bhoumik, W. Zhang, L. H. Wang *et al.*, RACK1
874 mediates activation of JNK by protein kinase C. *Mol. Cell* **19**, 309-320 (2005).
- 875 73. M. Sharma, V. Gadang, A. Jaeschke, Critical role for mixed-lineage kinase 3 in
876 acetaminophen-induced hepatotoxicity. *Mol. Pharmacol.* **82**, 1001-1007 (2012).
- 877 74. N. G. Brukman, S. Y. Nuñez, L. D. C. Puga Molina, M. G. Buffone, A. Darszon *et al.*,
878 Tyrosine phosphorylation signaling regulates Ca²⁺ entry by affecting intracellular pH
879 during human sperm capacitation. *J. Cell Physiol.* **234**, 5276-5288 (2019).
- 880 75. M. Lesort, R. S. Jope, G. V. Johnson, Insulin transiently increases tau phosphorylation:
881 involvement of glycogen synthase kinase-3beta and Fyn tyrosine kinase. *J. Neurochem.*
882 **72**, 576-584 (1999).

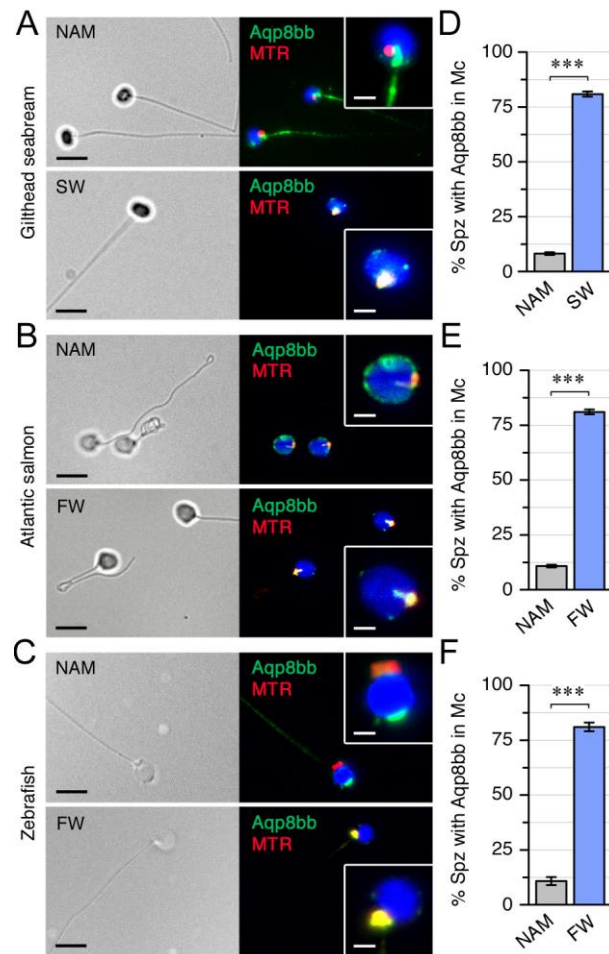


Fig. 1. The piscine Aqp8bb peroxiporin is transported to the mitochondria during spermatozoon motility activation. (A-C) Representative bright field images (left panels) and immunodetection (right panels) of Aqp8bb (green) in immotile (diluted in NAM) and activated spermatozoa of SW and FW spawning teleosts, using species-specific Aqp8bb antibodies. The mitochondria are labelled with MTR (red), whereas the spermatozoa nucleus are counterstained with DAPI (blue). Colocalized signals in mitochondria are yellow. Scale bars: 5 μ m (insets, 1 μ m). (D-E) Percentage of spermatozoa showing Aqp8bb mitochondrial localization after incubation in NAM or upon activation in SW or FW in each species. Data are the mean \pm SEM ($n = 4-5$ fish in A and B, and $n = 3$ pools of 5 different males each in C). Significance was measured by an unpaired Student's t -test with respect to immotile sperm. *** $P < 0.001$.

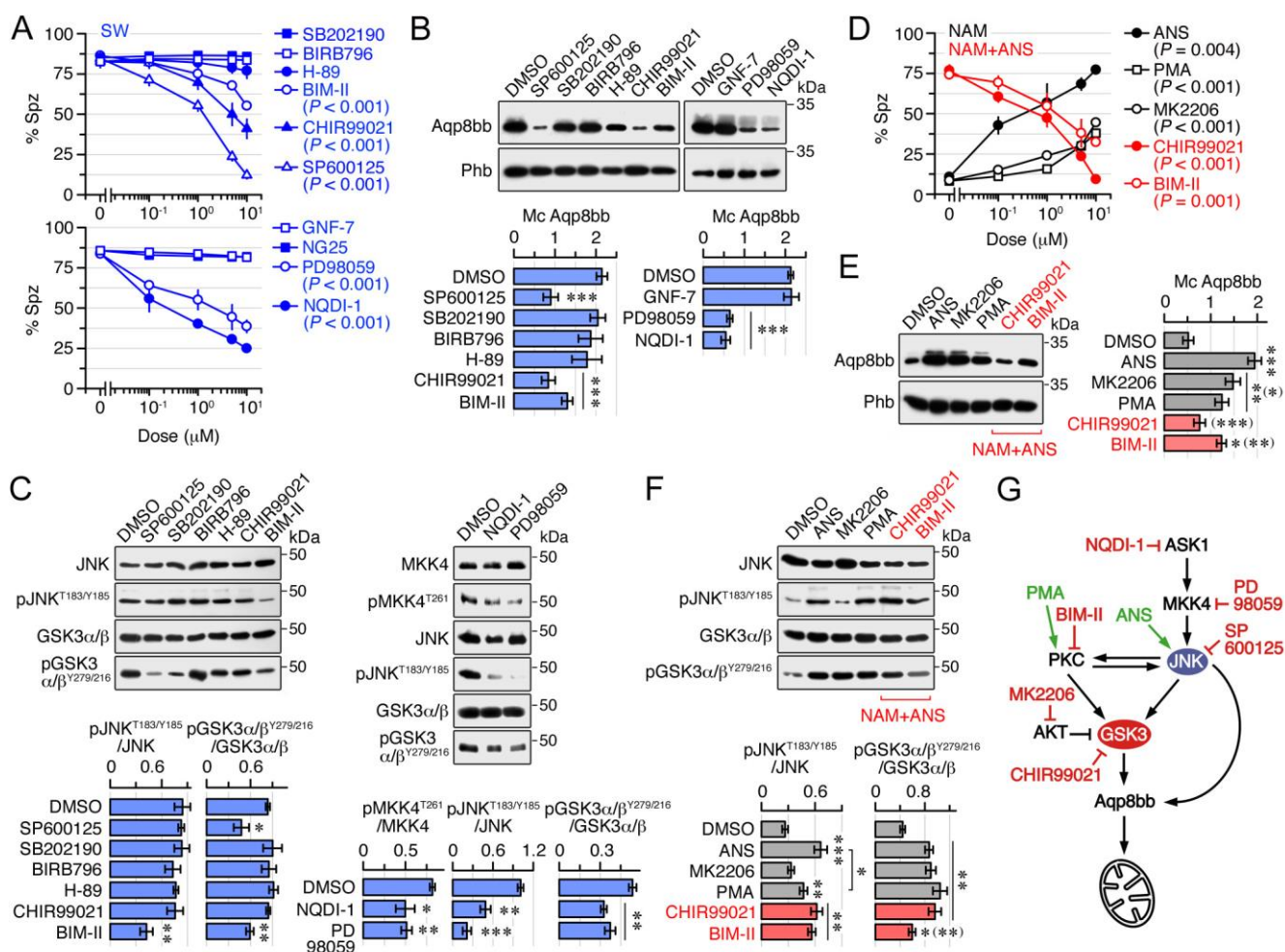


Fig. 2. Pharmacological identification of the major signal transduction pathways involved in Aqp8bb mitochondrial trafficking in seabream spermatozoa. (A) Dose-response inhibition of the percentage of activated spermatozoa showing Aqp8bb and MTR mitochondrial colocalization after treatment with DMSO alone (vehicle) or containing different protein kinase inhibitors determined by immunofluorescence microscopy. (B) Representative Aqp8bb immunoblots in mitochondrial extracts (upper panels), and corresponding quantitation normalised to Phb (lower panels), from sperm in A treated with 10 μM of the different drugs. (C) Total and phosphorylated JNK and GSK3 representative immunoblots (upper panels) in sperm from B, and densitometric analysis of kinase phosphorylation normalized to the corresponding total kinase blot (lower panels). (D, E) Activation of mitochondrial Aqp8bb trafficking in immotile spermatozoa maintained in NAM and exposed to activators of JNK (ANS), PKC (PMA) or GSK3 (MK2206) (black color) determined by immunofluorescence microscopy (D) and immunoblotting (E). Inhibition of ANS (10 μM)-induced Aqp8bb transport by inhibitors of GSK3 (CHIR99021) and PKC (BIM-II) is shown in red color. (F) MKK4, JNK and GSK3 activation in sperm treated as in D. (G) Proposed model of the JNK and GSK3 signaling pathways controlling Aqp8bb mitochondrial transport in activated seabream spermatozoa. The kinase inhibitors (red color) and activators (green color) used are indicated. In panels A-F, data (mean ± SEM; n = 3-7 fish) were statistically analyzed by one-way ANOVA (P-values for each compound are indicated in A and D). ***P < 0.001; **P < 0.01; *P < 0.05, with respect to control spermatozoa (treated with DMSO vehicle) or as indicated in brackets, or with respect to sperm treated with ANS alone (E and F in parenthesis).

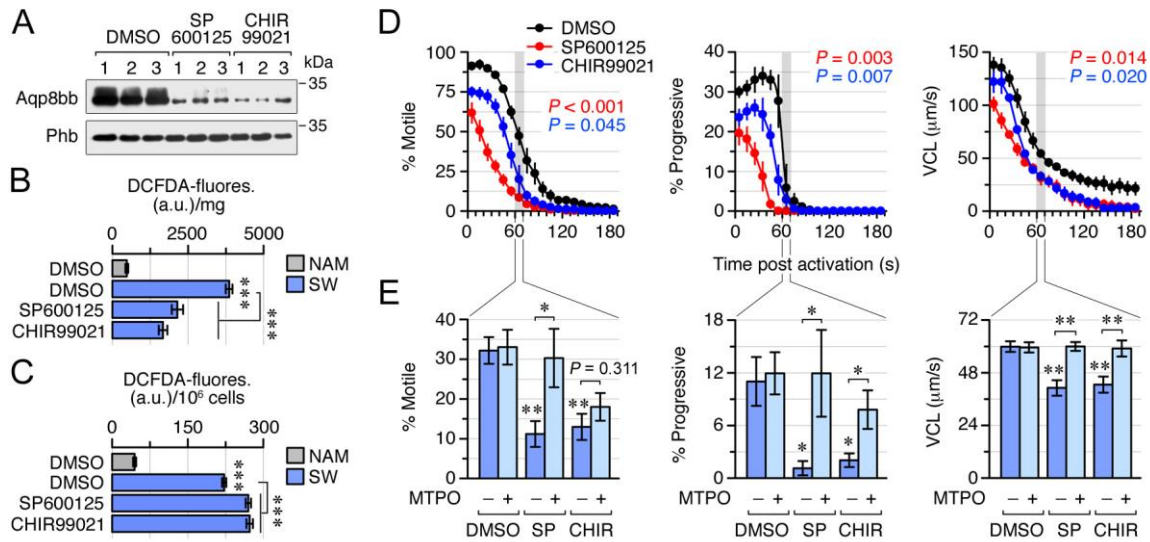


Fig. 3. JNK and GSK3 inhibition prevents Aqp8bb insertion into the seabream spermatozoa inner mitochondrial membrane upon SW activation. (A) Aqp8bb immunoblot in the inner mitochondrial membrane from SW-activated spermatozoa ($n = 3$ fish) exposed or not to 10 μM of the JNK (SP600125) and GSK3 (CHIR99021) inhibitors. Phb was used as a marker for even loading. (B) H_2O_2 uptake (mean \pm SEM, $n = 6$ fish) by mitochondria isolated from NAM and SW spermatozoa treated with or without the inhibitors. (C) ROS levels (mean \pm SEM, $n = 8$ fish) in spermatozoa treated as in B. Statistical differences were measured by one-way ANOVA. *** $P < 0.001$, with respect to NAM or SW-activated sperm not treated with the inhibitors, or as indicated in brackets. (D) Percentage of motility and progressivity, and curvilinear velocity (VCL), of spermatozoa (mean \pm SEM, $n = 4$ fish) treated with DMSO in the presence or absence of SP600125 and CHIR99021. Statistical differences with respect to control spermatozoa (only during the first 60 s for motility and progressivity) were determined by the Mann-Whitney U test (P -values indicated in each panel). (E) Effect of the mitochondria-targeted antioxidant Mito-TEMPO (MTPO; 50 μM) on the SP600125 (SP) or CHIR99021 (CHIR) inhibition of sperm kinetics (mean \pm SEM, $n = 7$ fish) at 60-70 s post-activation (marked with a grey bar in D). Data are statistically analyzed by one-way ANOVA (minus MTPO), and by the unpaired Student's t -test between sperm untreated and treated with MTPO. * $P < 0.05$; ** $P < 0.01$; *** $P < 0.001$, with respect to non-treated sperm, or as indicated in brackets.

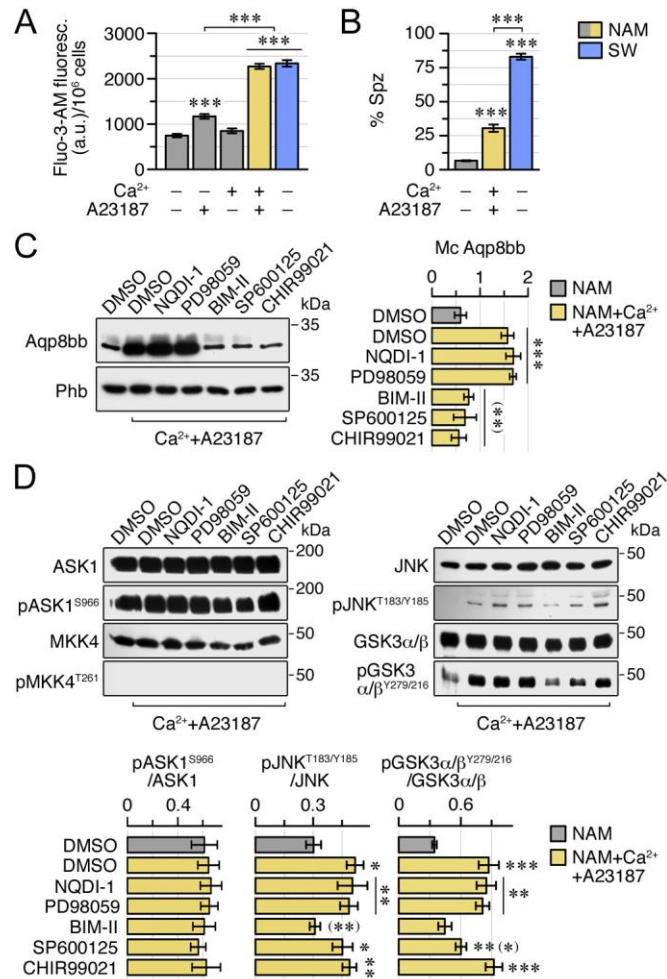


Fig. 4. An intracellular Ca²⁺ surge partially drives Aqp8bb transport to the mitochondrion in non-activated seabream spermatozoa. (A) Intracellular Ca²⁺ levels in sperm maintained in NAM and treated with 3 mM Ca²⁺ and/or 10 μM of the Ca²⁺ ionophore A23187, and in SW-activated sperm. (B) Percentage of spermatozoa showing Aqp8bb mitochondrial localization after exposure to Ca²⁺ and A23187 in NAM, or upon activation in SW. (C) Representative immunoblot of mitochondrial Aqp8bb (left panel), and corresponding quantitation normalised to Phb (right panel), from sperm incubated with or without Ca²⁺ and A23187 in NAM, and treated with 10 μM of different kinase inhibitors. (D) Total and phosphorylated ASK1, MKK4, JNK and GSK3α/β representative immunoblots (upper panels) in spermatozoa treated as in C. Lower panels depict the densitometric analysis of kinase phosphorylation normalized to the corresponding band from the total kinase blot. Data are the mean ± SEM (*n* = 4-6 fish) and are statistically analyzed by one-way ANOVA. ****P* < 0.001; ***P* < 0.01; **P* < 0.05, with respect to non-treated sperm, or treated with Ca²⁺+A23187 without inhibitors (in parenthesis), or as indicated in brackets.

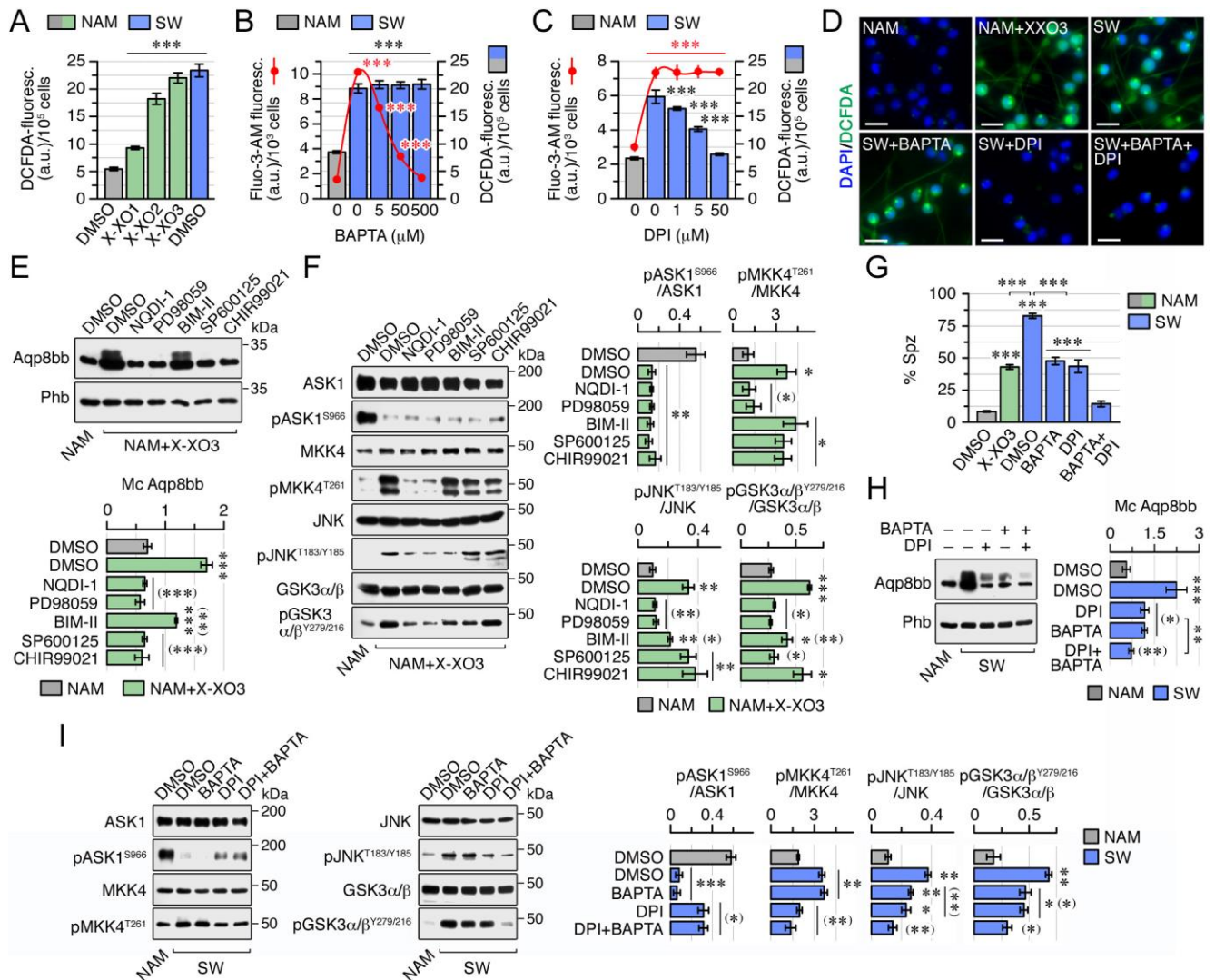


Fig. 5. Oxidative stress-induced Aqp8bb mitochondrial transport in seabream spermatozoa. (A) ROS levels in immotile sperm treated with increasing doses of X-XO (X-XO1, X-XO2 and X-XO3), and in SW-activated spermatozoa. (B, C) Intracellular Ca^{2+} (red line) and ROS levels (bars) in non-activated and activated sperm in the presence of BAPTA (B) or DPI (C). (D) Epifluorescence photomicrographs of non-activated and activated spermatozoa treated with X-XO3, 500 μM BAPTA, 50 μM DPI, or BAPTA+DPI, and labelled with the CM- H_2DCFDA dye (green). Nuclei are counterstained with DAPI (blue). Scale bars, 5 μm . (E) Immunoblot of mitochondrial Aqp8bb in sperm maintained in NAM and exposed to X-XO3 (upper panel), in the presence or absence of 10 μM of kinase inhibitors, and corresponding quantitation normalised to Phb (lower panel). (F) Total and phosphorylated ASK1, MKK4, JNK and GSK3 α/β immunoblots (left panels), and densitometric analysis of phosphorylated forms normalized to the corresponding non-phosphorylated bands (right panels), in spermatozoa treated as in E. (G) Percentage of spermatozoa showing Aqp8bb in mitochondria after treatment with X-XO3 in NAM, or upon activation in SW with or without BAPTA and/or DPI. (H) Immunoblot of mitochondrial Aqp8bb in immotile sperm or activated in SW with or without BAPTA and/or DPI (left panels) and quantitation normalised to Phb (right panel). (I) Immunoblots of kinase activation in sperm treated as in H (left panels) and quantitation of phosphorylated forms. In all panels, data are displayed as mean \pm SEM ($n = 4-6$ fish) and are statistically analyzed by one-way ANOVA. *** $P < 0.001$; ** $P < 0.01$; * $P < 0.05$, with respect to non-treated spermatozoa in NAM, spermatozoa exposed to NAM plus X-XO3 or SW without inhibitors (in parenthesis), or as indicated in brackets (G and E).

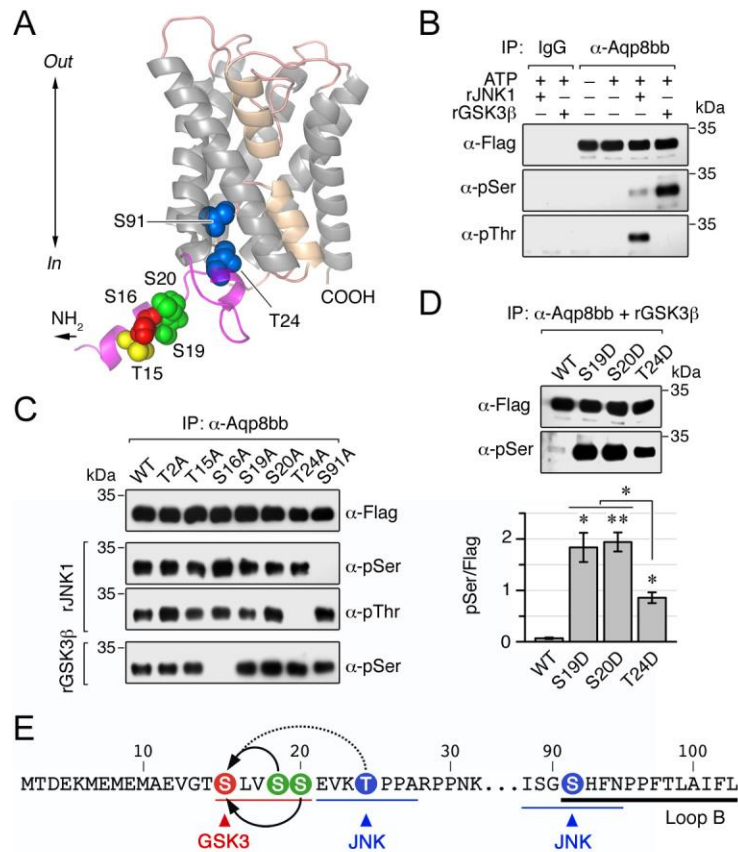


Fig. 6. Phosphorylation of seabream Aqp8bb by GSK3 and JNK *in vitro*. (A) Mirrored lateral view of seabream Aqp8bb, rendered by MacPymol using orthologous *Pichia pastoris* Aqy1 (3ZOJ) as the structure mask. The render shows all potential Ser and Thr phosphorylation sites (spacefill) in the N-terminus (magenta), except Thr², with Ser⁹¹ in the cytoplasmic loop B. The predicted phosphorylation sites by GSK3 (Ser¹⁶, Ser¹⁹ and Ser²⁰) and proline-directed kinase (Thr²⁴), such as JNK, are indicated in red and blue color, respectively. The Ser⁹¹ shows low mixed score for GSK3/proline-directed kinase phosphorylation. (B) Immunoblot of Ser and Thr phosphorylation of immunoprecipitated Aqp8bb-Flag from transfected HEK293T cells by recombinant JNK1 (rJNK1; 0.11 μM) or GSK3β (rGSK3β; 0.17 μM), in the presence or absence of 200 μM ATP. Immunoprecipitation with rabbit immunoglobulin G (IgG) is used as control. (C) *In vitro* phosphorylation of wild-type Aqp8bb-Flag (WT) and single mutants determined as above. A representative blot of two independent experiments is shown. (D) Immunoblot of Ser¹⁶ phosphorylation in Aqp8bb-Flag-WT and Aqp8bb-S19D, -S20D and -T24D phosphomimetic mutants by rGSK3β (0.08 μM). The right panel shows the corresponding quantitation (mean ± SEM; *n* = 3 independent experiments) of phosphorylated Aqp8bb-Flag normalised to the total immunoprecipitated protein. Data are statistically analyzed by one-way ANOVA. ***P* < 0.01; **P* < 0.05, with respect to the WT, or as indicated in brackets. (E) Schematic representation of the seabream Aqp8bb N-terminus and loop B showing potential priming sites (Ser¹⁹, Ser²⁰ and Thr²⁴) for Ser¹⁶ phosphorylation by rGSK3β (arrows). Consensus sequences for GSK3 and JNK phosphorylation are underlined in red and blue, respectively, whereas the corresponding target residues are indicated by arrowheads.

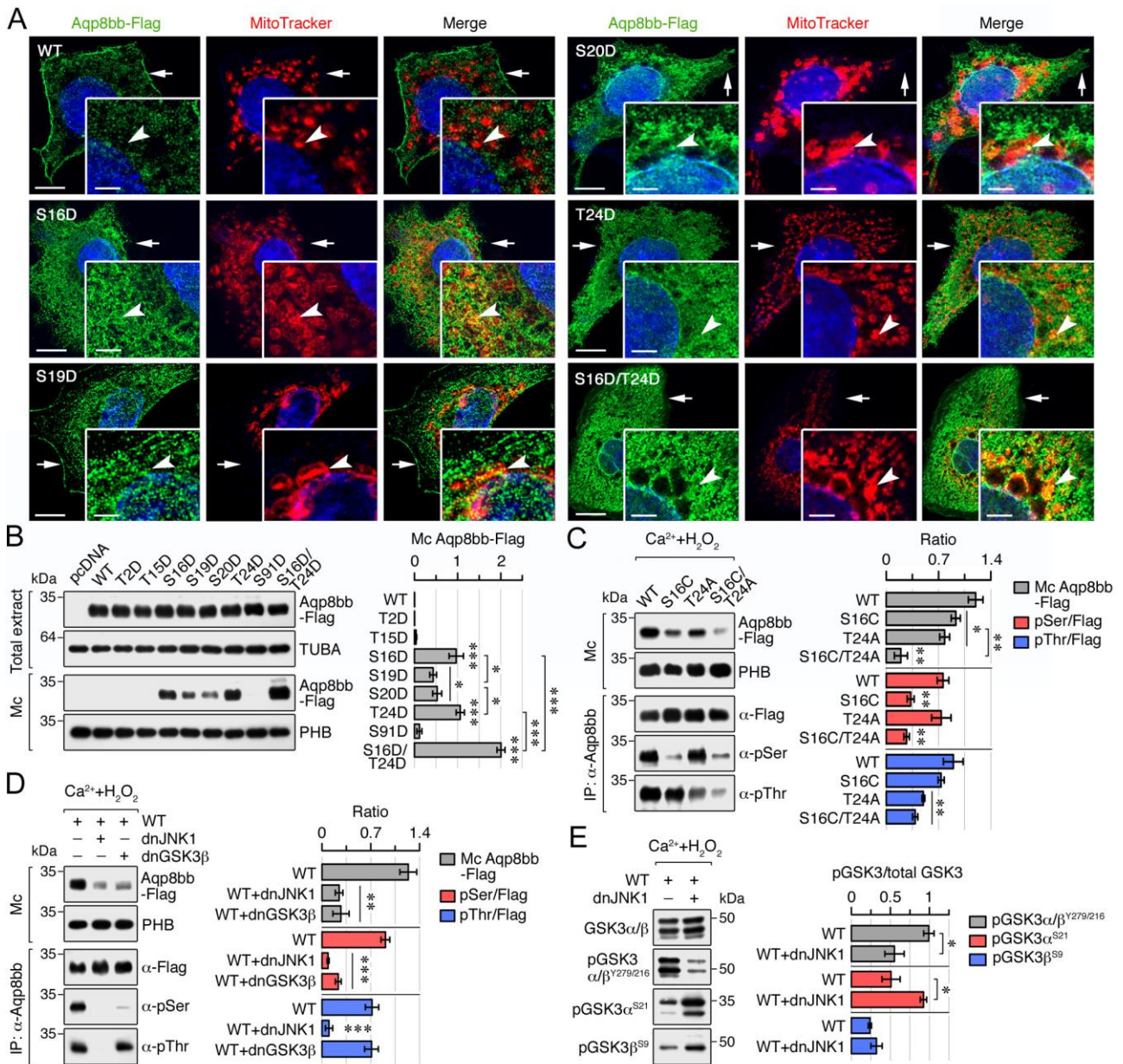


Fig. 7. Dual N-terminus phosphorylation of seabream Aqp8bb by GSK3 and JNK control mitochondrial channel transport in HepG2 cells. (A) Double staining of Aqp8bb-Flag (green) and mitochondria (MTR, red) in cells transiently expressing wild-type Aqp8bb-Flag (WT) or phospho-mimetic mutants as indicated. Arrows point to the plasma membrane, whereas arrowheads indicate co-localized signals in the mitochondria. Scale bars, 10 μm (insets 5 μm). (B) Representative immunoblot of total and mitochondrial Aqp8bb-Flag-WT and mutants, using tubulin (TUBA) and PHB as loading controls, respectively (left panels). Mitochondrial Aqp8bb-Flag quantitation is normalised to PHB (right panel). (C) Immunoblot of mitochondrial Aqp8bb-Flag-WT and -S16C, T24A and S16C/T24A mutant channels, and Ser and Thr phosphorylation of the corresponding immunoprecipitated proteins, in cells treated with Ca^{2+} and H_2O_2 . Right panels show the amount of each construct in the the mitochondria, normalised to PHB, and their Ser and Thr phosphorylation state normalised to the total immunoprecipitated protein. (D) Effect of coexpression of Aqp8bb-Flag-WT and dominant-negative forms of JNK1 and GSK3 β (dnJNK1 and dnGSK3 β , respectively) on the mitochondrial transport and Ser/Thr phosphorylation of the channel in cells treated as in C. (E) Immunoblot of non-activated and activated GSK3 in cells coexpressing Aqp8bb-Flag-WT and dnJNK1 and treated with Ca^{2+} and H_2O_2 (left panels), and densitometric analysis of phosphorylated GSK3 forms (right panel). In B-C, quantifications are displayed as mean \pm SEM ($n = 3$ separate experiments), and data are statistically analyzed by one-way ANOVA (B-D) or by an unpaired Student's t -test (E). *** $P < 0.001$; ** $P < 0.01$; * $P < 0.05$, with respect Aqp8bb-Flag-WT or as indicated in brackets.

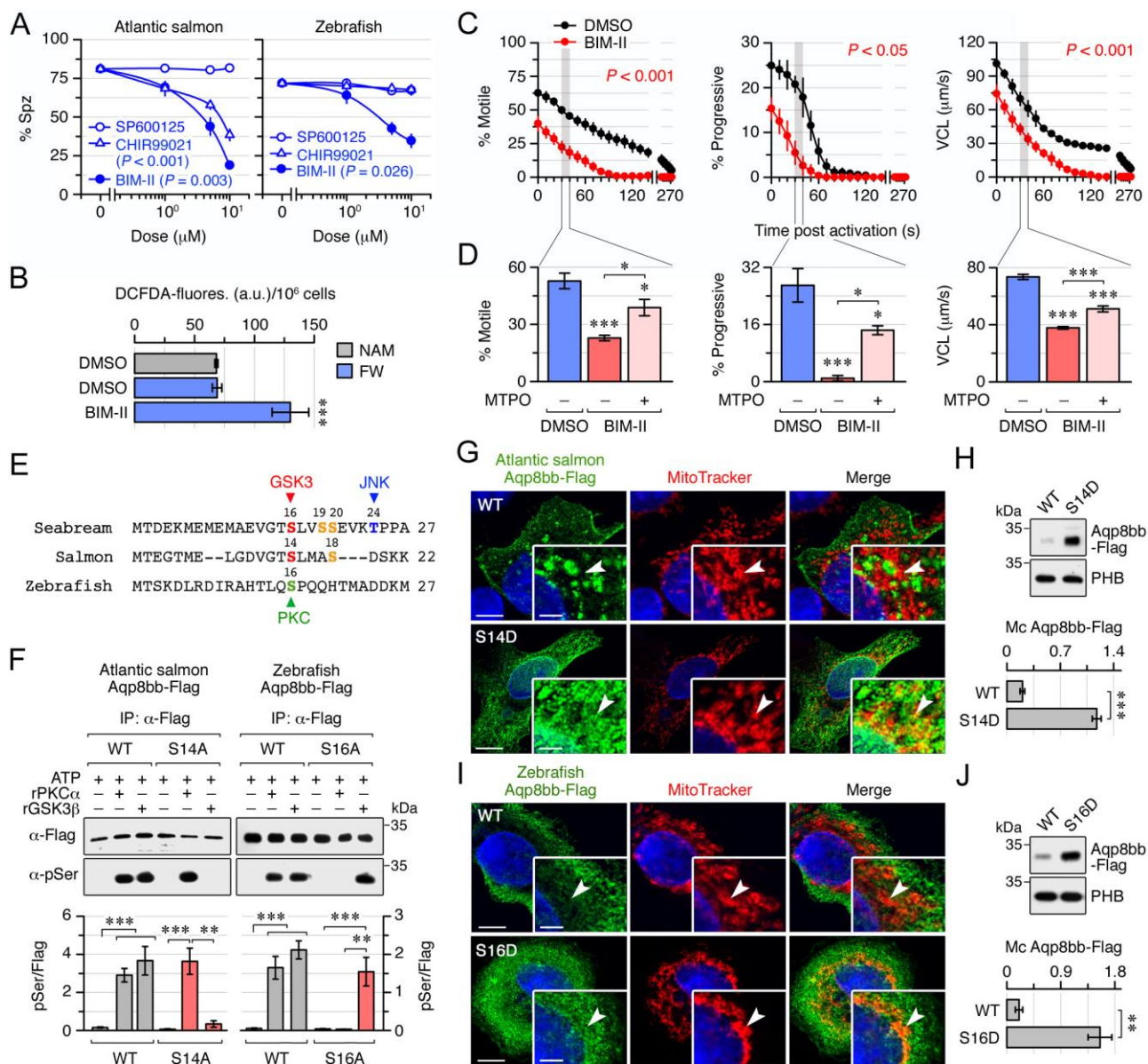


Fig. 8. Aqp8bb mitochondrial transport in FW spermatozoa is controlled by monophosphorylation of the N-terminus of the channel by PKC or GSK3. (A) Percentage of salmon and zebrafish spermatozoa (mean \pm SEM; $n = 4$ fish for salmon, and $n = 3$ pools of 5 fish for zebrafish) showing Aqp8bb mitochondrial localization after treatment with vehicle (DMSO), or JNK (SP600125), PKC (BIM-II) or GSK3 (CHIR99021) inhibitors. (B) ROS levels (mean \pm SEM; $n = 6$ fish) in immotile and activated zebrafish spermatozoa treated with vehicle or BIM-II. (C) Motility, progressivity and curvilinear velocity (VCL) of zebrafish activated spermatozoa (mean \pm SEM, $n = 7$ fish) treated with vehicle or BIM-II. P -values are calculated from the Mann-Whitney U test (during the first 60 s only for motility and progressivity). (D) Effect of Mito-TEMPO (MTPO; 50 μ M) on BIM-II inhibition of zebrafish sperm kinetics (mean \pm SEM, $n = 5$ fish) at 30-40 s post-activation (grey bar in C). Data in B and D are statistically analyzed by one-way ANOVA (*** $P < 0.001$; * $P < 0.05$, with respect to non-treated sperm). (E) Amino acid sequence alignment of seabream, salmon and zebrafish Aqp8bb N-terminus indicating the GSK3, PKC and JNK phosphorylation sites. (F) Immunoblot of Ser phosphorylation in salmon and zebrafish Aqp8bb-Flag-WT and -S14A and -S16A mutants, respectively, after phosphorylation *in vitro* by rPKC α (0.08 μ M) and rGSK3 β (0.17 μ M). Lower panels show the quantitation of phosphorylated channel normalised to total immunoprecipitated protein. (G, I) Aqp8bb-Flag and MTR double staining of HepG2 cells expressing salmon (G) or zebrafish (I) Aqp8bb-Flag-WT and phosphomimetic mutants. Arrowheads indicate co-localized signals in the mitochondria. Scale bars, 10 μ m (insets 5 μ m). (H, J) Immunoblots of Aqp8bb-Flag-WT and mutants in mitochondrial extracts from cells shown in G and I. Data in F, H and J are the mean \pm SEM of 3 separate experiments, and are statistically analyzed by one-way ANOVA (F) or an unpaired Student's t -test (H and J). *** $P < 0.001$; ** $P < 0.01$, as indicated in brackets.

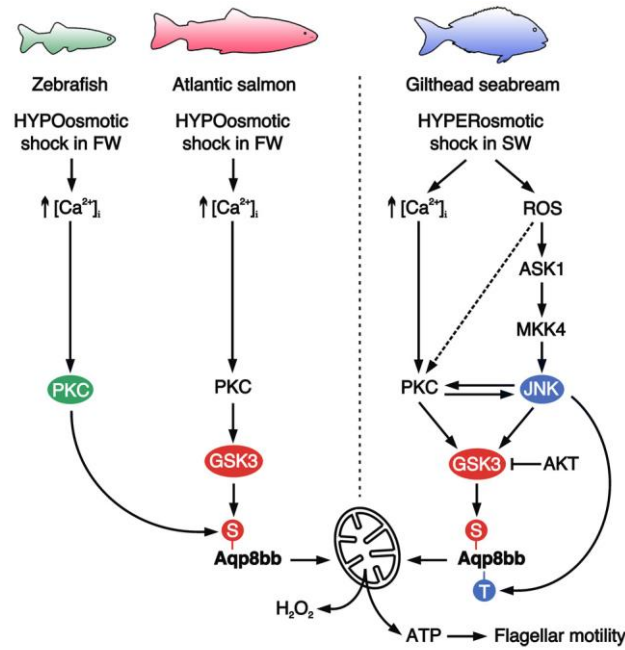


Fig. 9. A model for the evolution of the intracellular multiplier peroxiporin signal transduction pathway powering piscine spermatozoa. In spermatozoa from more primitive FW teleost lineages, such as in zebrafish and salmonids, a rise of intracellular Ca^{2+} ($[\text{Ca}^{2+}]_i$) upon activation in FW triggers the PKC-GSK3 signaling pathway, leading to the direct PKC (zebrafish) or GSK3 (Atlantic salmon) phosphorylation of N-terminal Aqp8bb residues, promoting rapid channel trafficking to the mitochondria. In modern marine teleosts such as the seabream, which release the sperm into SW, a cross talk between $[\text{Ca}^{2+}]_i$ -activated PKC and ROS-activated JNK and PKC signaling pathways converge to activate GSK3 with an additional JNK-mediated multiplier regulation of Aqp8bb mitochondrial trafficking to cope with a higher osmotic stress.



Supplementary Information for:

A multiplier peroxiporin signal transduction pathway powers piscine spermatozoa

François Chauvigné, Alba Ferré, Carla Ducat, Tom Hansen, Montserrat Carrascal, Joaquín Abián, Roderick Nigel Finn and Joan Cerdà

Joan Cerdà
Email: joan.cerda@irta.cat

This PDF file includes:

Supplementary text
Figures S1 to S10
Supplementary Materials and Methods
Tables S1 to S4
SI References

Supplementary Text S1

The Aqp8bb spermatozoon mitochondrial transport pathway can be replicated in human HepG2 cells. We transiently transfected the HepG2 cells with seabream Aqp8bb-Flag and exposed them to external 10 mM of Ca^{2+} and/or 100 μM H_2O_2 , which elicit maximum intracellular levels of the solutes (Fig. S8A). Immunolabelling of Aqp8bb-Flag in cells loaded with MitoTracker to stain mitochondria shows that both Ca^{2+} and H_2O_2 trigger the co-localization of Aqp8bb and MitoTracker signals, suggesting the activation of channel transport into the mitochondria (Fig. S8B). These observations are corroborated by Aqp8bb-Flag immunoblotting of mitochondrial extracts, which also show that when both compounds are present the accumulation of the channel in the mitochondria approximately doubles (Fig. S8C). This suggests that Ca^{2+} and H_2O_2 activate independent and additive signaling pathways in HepG2 cells controlling Aqp8bb trafficking as observed in seabream spermatozoa.

The stimulatory effect of Ca^{2+} on Aqp8bb mitochondrial transport in HepG2 cells is associated with the activation of GSK3 but not of JNK, whereas H_2O_2 triggers the activation of both JNK and GSK3 (Fig. S8D). When cells are exposed to both Ca^{2+} and H_2O_2 the activation of JNK is similar to that seen with H_2O_2 alone, while that of GSK3 is approximately the double with respect to that noted with Ca^{2+} or H_2O_2 (Fig. S8D). The inhibitory GSK3 $\alpha^{\text{S}21}$ phosphorylation is equally reduced by Ca^{2+} or H_2O_2 treatment, and this seems to decrease further using both compounds together (Fig. S8D), suggesting that Ca^{2+} and H_2O_2 increase GSK3 activity in HepG2 cells by enhancing and decreasing Gsk3 $\alpha/\beta^{\text{Y}279/\text{216}}$ and GSK3 $\alpha^{\text{S}21}$ phosphorylation, respectively.

The inhibition of PKC, JNK and GSK3 during Ca^{2+} and/or H_2O_2 -triggered Aqp8bb mitochondrial transport, using BIM-II, SP600125 and CHIR99021, respectively, show that PKC and GSK3, but not JNK, are essential for Ca^{2+} -mediated partial channel transport (Fig. S8E), possibly through PKC activation of GSK3, since only PKC inhibition decreased GSK3 $\alpha/\beta^{\text{Y}279/\text{216}}$ phosphorylation (Fig. S8F). In contrast, JNK and GSK3, but not PKC, are involved in the stimulatory effect of H_2O_2 on Aqp8bb trafficking, through JNK activation, which increases GSK3 $\alpha/\beta^{\text{Y}279/\text{216}}$ phosphorylation (Fig. S8 E and F). Interestingly, $\text{Ca}^{2+} + \text{H}_2\text{O}_2$ -triggered Aqp8bb trafficking is strongly reduced after JNK and GSK3 inhibition, but only partially blocked by the PKC inhibitor (Fig. S8E). However, both JNK and PKC inhibitors reduced GSK3 activation to a similar extent (Fig. S8F), which suggest a direct action of JNK driving Aqp8bb transport, in addition to that mediated by GSK3, as found in seabream sperm.

Together, these data indicate that the same PKC-GSK3 and JNK-GSK3 signaling cascades that control Aqp8bb mitochondrial transport in the seabream spermatozoon can be replicated in HepG2 cells (Fig. S8G), except that in these human cells the cross-talk between PKC and JNK does not occur.

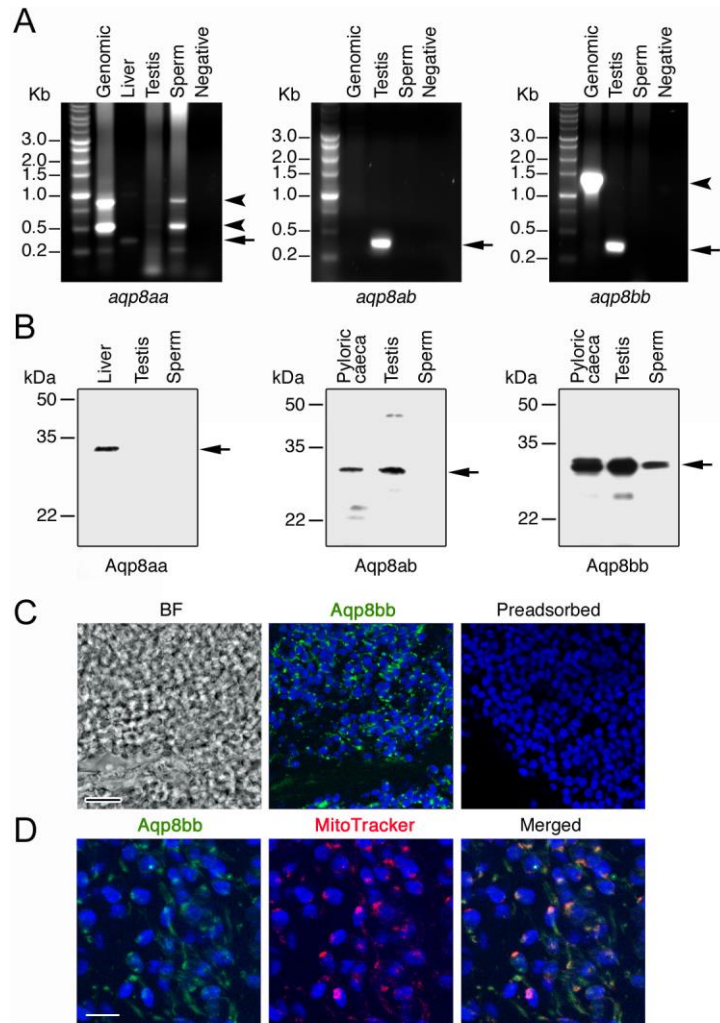


Fig. S1. The Atlantic salmon (*Salmo salar*) Aqp8bb peroxiporin, but not the Aqp8aa or -8ab paralogs, is expressed in spermatozoa. (A) RT-PCR analysis of *aqp8aa*, -8ab and -8bb expression in different tissues of adult fish. Genomic DNA is used as positive controls, whereas the absence of RT during cDNA synthesis (Negative) is the negative control. The arrows indicate transcripts, whereas the arrowheads indicate genomic products. The size (kb) of PCR products and molecular markers are indicated on the left. (B) Immunoblots for Aqp8aa, -8ab and -8bb in different tissues using Atlantic salmon paralog-specific antibodies (Table S4) show that only the Aqp8bb paralog is expressed in spermatozoa. Arrows indicate aquaporin monomers. Molecular mass markers (kDa) are on the left. (C) Representative brightfield (BF) and immunofluorescence microscopy images of Aqp8bb immunolocalization (green) in testicular spermatozoa of Atlantic salmon using the Aqp8bb-specific antibody. Control sections incubated with preabsorbed antisera are negative (right). (D) Double staining for Aqp8bb (green) and MTR (red) shows that the channel does not localize in the mitochondria in most of the intratesticular spermatozoa. In C and D, nuclei are stained with DAPI (blue). Scales bars, 10 μ m (C), 5 μ m (D).

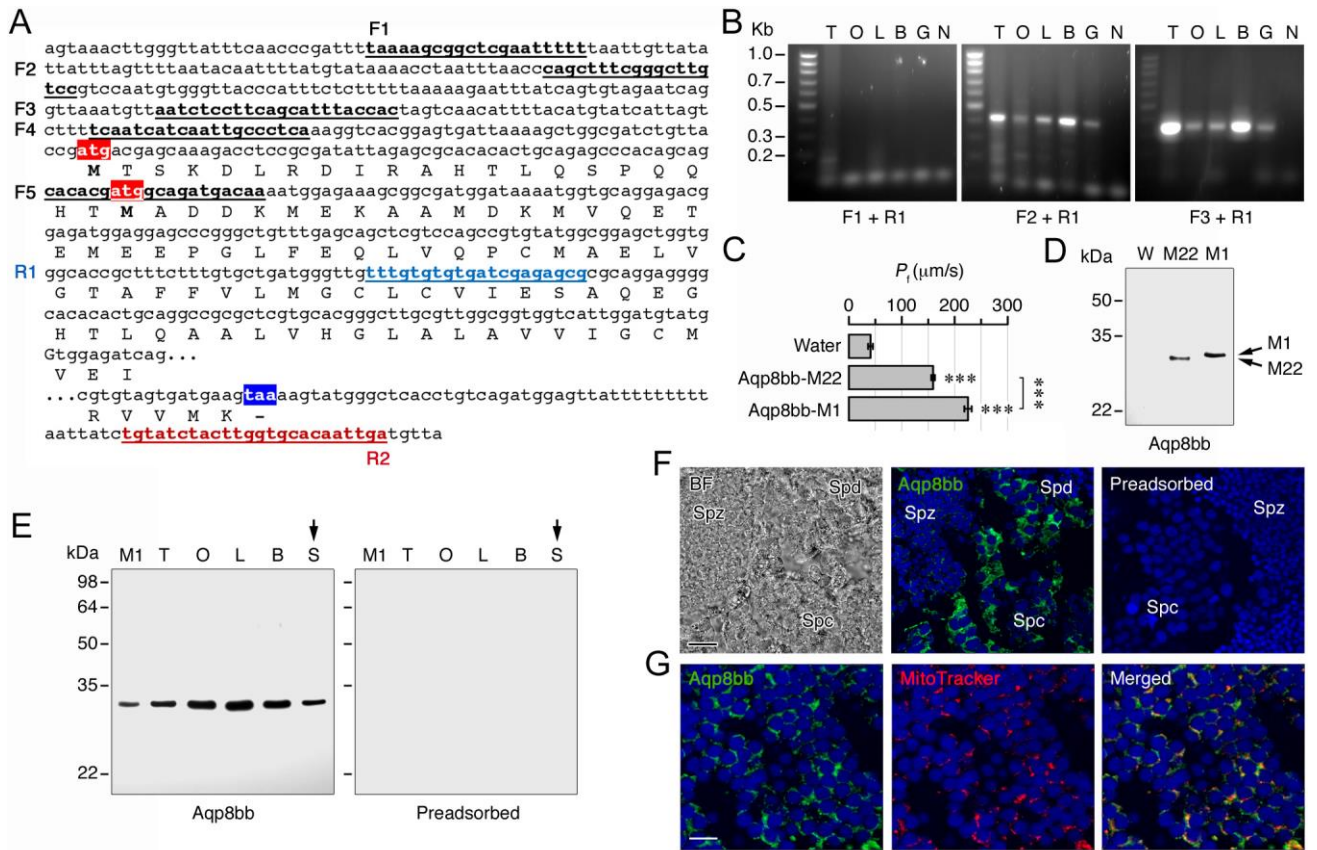


Fig. S2. Cloning and functional characterization of the complete zebrafish Aqp8bb paralog with an extended N-terminal domain. (A) Partial genomic sequence of exon 1 and upstream region, and of the end of exon 5 and downstream region, of the zebrafish *aqp8bb* locus (Ensembl chromosome: Zv9:3:18301156:18305325). The deduced amino acid sequence is shown below; two potential translation initiation codons (M1 and M22) are highlighted in red, whereas the stop codon is in blue. (B) Partial amplification of the 5' end *aqp8bb* mRNA (containing the N-terminus of the deduced protein) in different adult tissues (T, testis; O, ovary; L, liver; B, brain; G, gills) using different forward primers underlined in bold (F1, F2 and F3) and a reverse primer underlined in blue (R1), mapped in a, as indicated in each panel. The N indicates absence of RT during cDNA synthesis. The results show the amplification of a single mRNA species with F2 and F3 primers in all tissues examined, suggesting the absence of 5' end mRNA splicing. (C) Osmotic water permeability (P_f) of *Xenopus laevis* oocytes injected with water (control) or expressing Aqp8bb cRNAs (15 ng) bearing the translation initiation codons at M1 or M22. The corresponding full-length cDNAs are cloned using primers F4 or F5 and R2 (red color), mapped in A, from testis total RNA. Data are the mean \pm SEM ($n = 14-15$ oocytes), and are statistically analyzed by one-way ANOVA. *** $P < 0.001$, with respect to water-injected oocytes or as indicated in brackets. (D) Immunoblot of control, Aqp8bb-M1 or -M22 oocytes using a zebrafish Aqp8bb specific antibody raised against the C-terminus (Table S1). The results in C and D indicate that both Aqp8bb-M1 and Aqp8bb-M22 are expressed at approximately the same level, while the M1 channel is more permeable than M22, suggesting that the latter cDNA sequence previously reported (GenBank accession no. NM_001114910), is lacking part of the N-terminus. (E) Immunoblot analysis of Aqp8bb in different adult tissues (as in B; S, non-activated intratesticular sperm, arrow) reveals a single reactive band with an apparent molecular mass similar to that of the Aqp8bb-M1 polypeptide (lane M1 in the blot) (left panel). A duplicated blot was run in parallel using the primary antibody preadsorbed with the antigenic peptide to test for specificity (right panel). The data suggest the absence of alternative translation initiation sites *in vivo*, and therefore, the Aqp8bb-M1 cDNA most likely encodes for the complete zebrafish Aqp8bb paralog. In D and E, molecular mass markers (kDa) are on the left. (F) Representative brightfield and immunofluorescence microscopy images of Aqp8bb immunolocalization (green) in the testis. Control sections incubated with preabsorbed antisera are negative (right). (G) Double immunostaining for Aqp8bb (green) and MTR (red) shows that the channel is expressed in the intratesticular spermatozoa but that it does not localize in the mitochondria in most of the cells. In F and G, nuclei are stained with DAPI (blue). Scale bars, 10 μ m (F), 5 μ m (G). Spc, spermatocytes; Spd, Spermatids; Spz, spermatozoa.

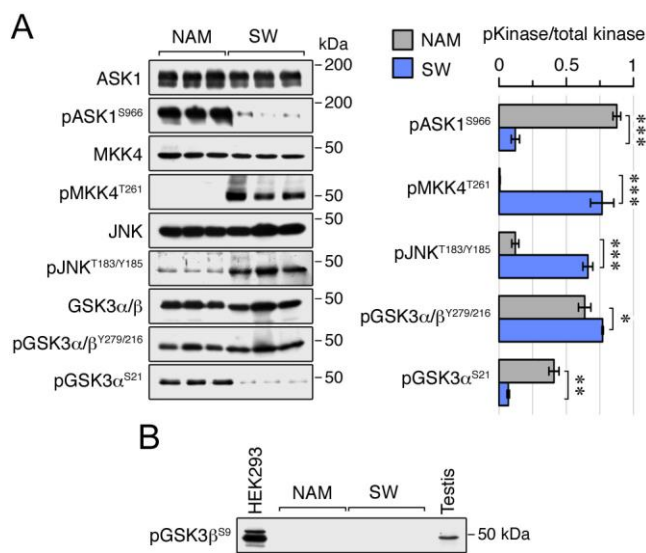


Fig. S3. Immunoblot analysis of kinase phosphorylation in seabream spermatozoa upon motility activation in SW. (A) Total and phosphorylated Ask1, Mkk4, Jnk and Gsk3 immunoblots in sperm from 3 males maintained in NAM or activated in SW (left panels). The right panel shows the densitometric analysis (mean \pm SEM; $n = 3$ fish) of kinase phosphorylation normalized to the corresponding band from the total kinase blot. Statistical differences were determined by the unpaired Student *t* test. *** $P < 0.001$; ** $P < 0.01$; * $P < 0.05$, with respect to sperm in NAM. (B) Immunoblotting detection of pGsk3β^{S9} in HEK293 cultured cells and seabream testis, but not in sperm either in NAM or SW ($n = 3$ fish each), suggesting that phosphorylation of Gsk3β possibly does not play a role during sperm activation in seabream spermatozoa.

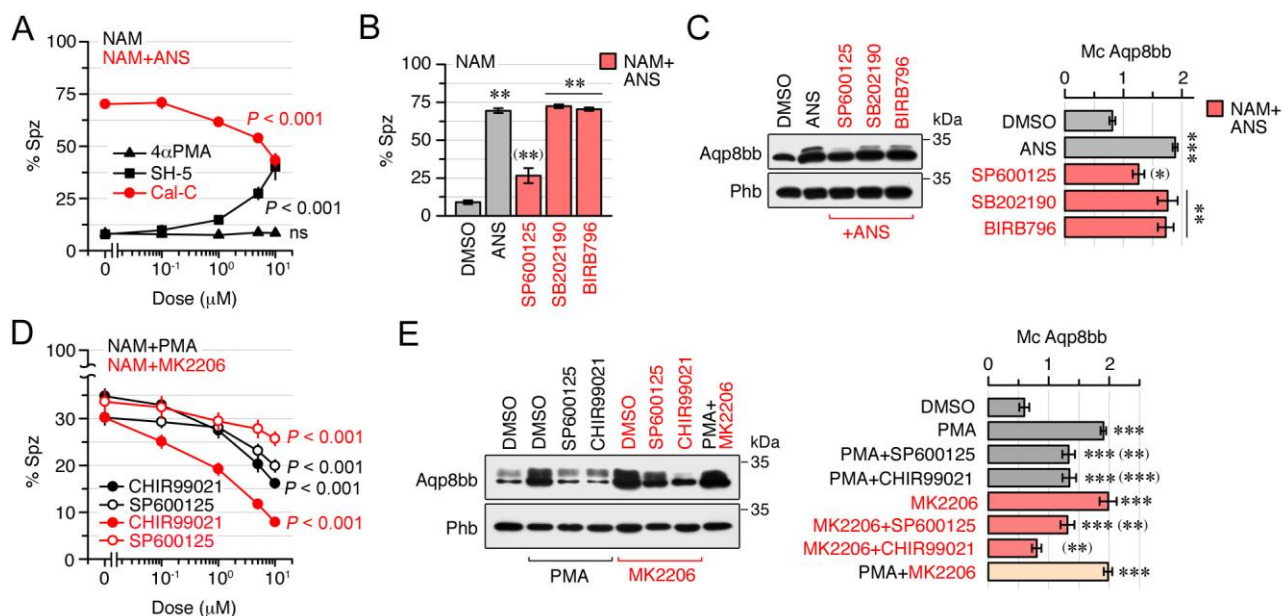


Fig. S4. Additional modulators of Aqp8bb mitochondrial trafficking in immotile seabream spermatozoa. (A) Dose-response activation or inhibition of Aqp8bb mitochondrial transport, determined by immunofluorescence microscopy. Sperm maintained in NAM was exposed to an inhibitor of AKT/PKB (SH-5), or to the 4- α -PMA (4 α -PMA) negative control (black color), while ANS (10 μ M)-treated sperm in NAM is incubated with a PKC inhibitor (Cal-C) (red color). (B, C) Effect of the JNK inhibitor SP600125, and two p38 MAPK inhibitors (SB202190 and BIRB796) (10 μ M) on ANS-induced Aqp8bb mitochondrial trafficking in spermatozoa determined by immunofluorescence microscopy (B) and immunoblotting of mitochondrial extracts (C). The right panel in C is the corresponding quantitation of mitochondrial Aqp8bb normalised to Phb. (D, E) Effect of JNK and GSK3 inhibitors (SP600125 and CHIR99021, respectively) on PMA and/or MK2206-induced Aqp8bb trafficking determined as above. In all panels, data are the mean \pm SEM ($n = 3-5, 3, 3, 3-5,$ and 6 different fish, in A, B, C, D and E, respectively). Statistical differences are measured by one-way ANOVA (P -values for each compound are indicated in a and d). *** $P < 0.001$; ** $P < 0.01$, with respect to non-treated spermatozoa in NAM, or with respect to sperm treated with ANS, PMA or MK2206 alone (in parenthesis).

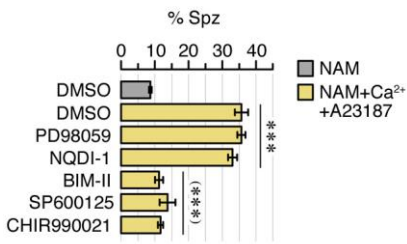


Fig. S5. Inhibition of Ca²⁺-induced Aqp8bb trafficking in seabream spermatozoa. Effect of different kinase inhibitors (10 μ M) on the percentage of immotile seabream spermatozoa showing Aqp8bb mitochondrial localization after incubation in Ca²⁺+A23187 determined by immunofluorescence microscopy. Data (mean \pm SEM; $n = 5$ fish) are statistically analyzed by one-way ANOVA. *** $P < 0.001$, with respect to untreated sperm in NAM, or treated with DMSO alone in Ca²⁺+A23187 (parenthesis).

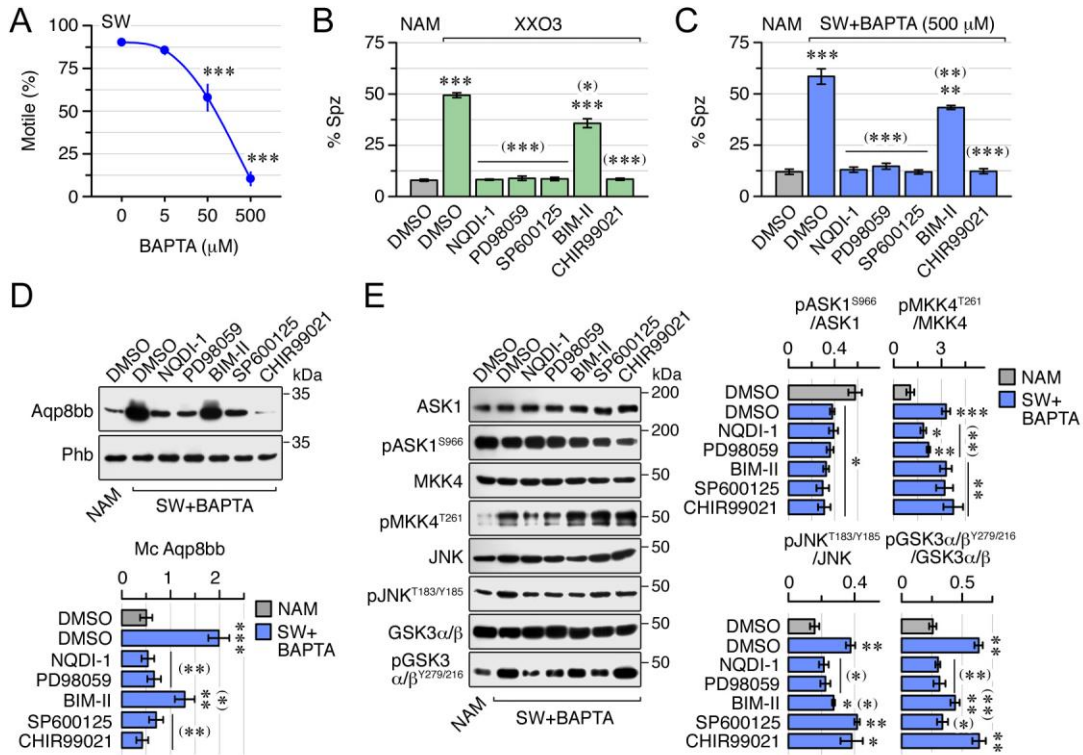


Fig. S6. (A) Percentage of motility of seabream sperm activated in SW containing increasing doses of BAPTA. (B, C) Percentage of spermatozoa in NAM and after treatment with XXO3 (B) or SW+BAPTA (C) showing Aqp8bb in the mitochondrion, and after treatment with kinase inhibitors (10 μ M). (D) Representative immunoblot of Aqp8bb in the mitochondria of sperm activated in SW+BAPTA in the presence of kinase inhibitors as in C (upper panels), and corresponding quantitation normalized to Phb (lower panel). (E) Total and phosphorylated ASK1, MKK4, JNK and GSK3 α/β representative immunoblots (left panels), and densitometric analysis of phosphorylated forms normalized to the corresponding non-phosphorylated bands (right panels), in spermatozoa treated as in C and D. In all panels, data are the mean \pm SEM ($n = 7$ fish in A, $n = 5$ fish in B and C, $n = 6$ fish in D, and $n = 4$ in E), and are statistically analyzed by one-way ANOVA. *** $P < 0.001$; ** $P < 0.01$; * $P < 0.05$, with respect to untreated sperm in NAM, or treated with DMSO alone in XXO3 or SW+BAPTA (in parenthesis).

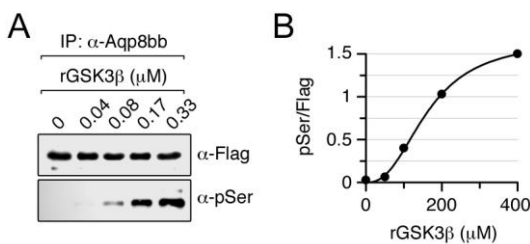


Fig. S7. (A) Dose-response in Ser phosphorylation of immunoprecipitated wild-type Aqp8bb-Flag after incubation with increasing amounts of rGSK3 β and 200 μ M ATP. (B) Corresponding quantitation of Aqp8bb-Flag Ser phosphorylation normalized to the total immunoprecipitated protein. Data are the mean of 2 independent experiments.

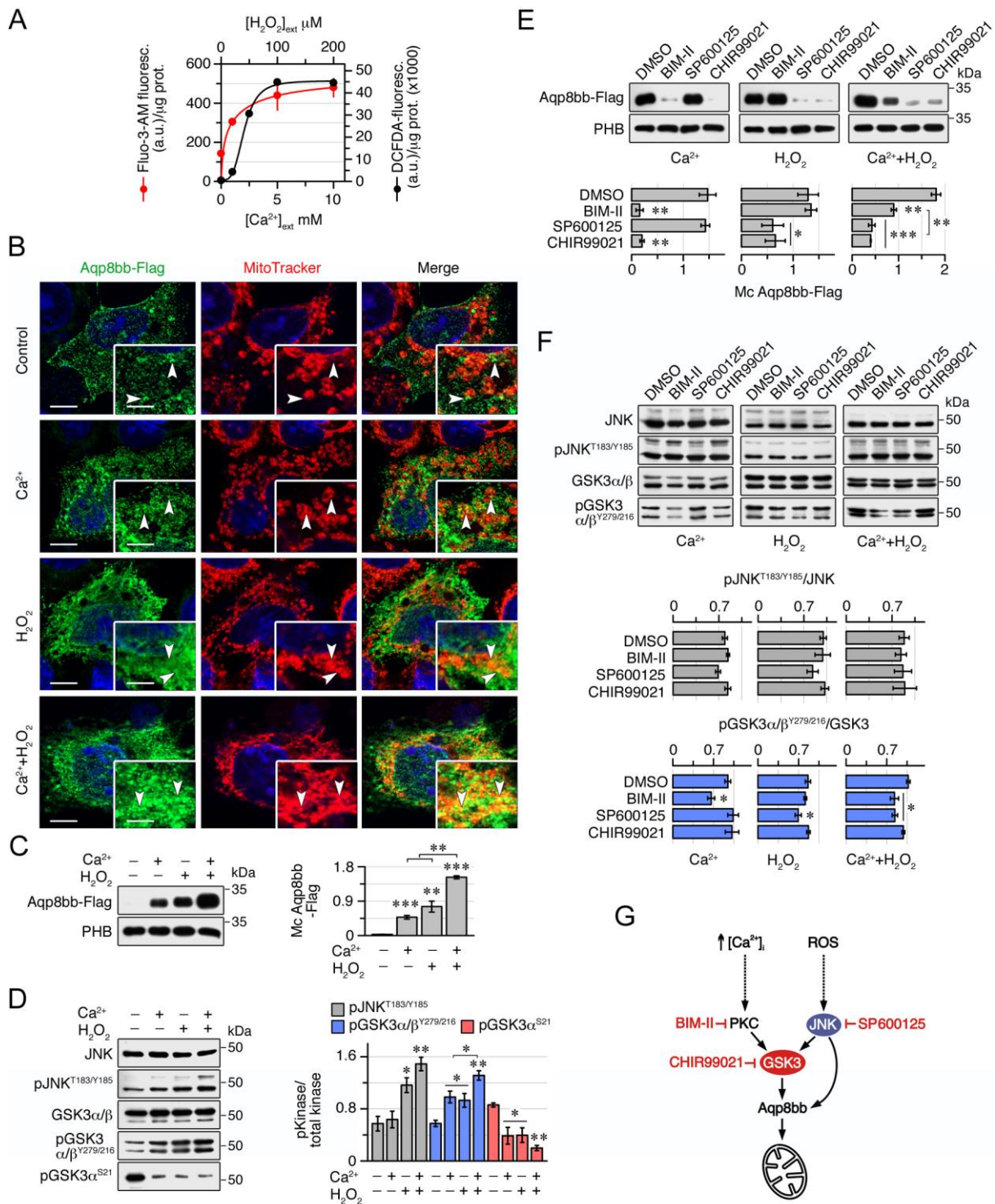


Fig. S8. Ca^{2+} - and ROS-mediated signaling pathways controlling Aqp8bb mitochondrial transport in seabream spermatozoa can be replicated in human HepG2 culture cells. (A) Dose-response increment (mean \pm SEM of 6-8 replicates from one experiment) of $[\text{Ca}^{2+}]_i$ (red line) and ROS levels (black line) in HepG2 cells in response to extracellular Ca^{2+} and H_2O_2 . (B) Double staining of Aqp8bb-Flag and mitochondria in non-treated transfected HepG2 cells or after treatment with Ca^{2+} (10 mM) and/or H_2O_2 (100 μM). Arrowheads indicate co-localized signals. Scale bars, 10 μm (5 μm , insets). (C) Immunoblot of mitochondrial Aqp8bb-Flag in cells treated as in B (left panel), and corresponding quantitation normalised to PHB (right panel). (D) JNK and GSK3 immunoblots (left), and densitometric analysis of phosphorylated forms normalised to the corresponding non-phosphorylated bands (right), in cells treated as in B. (E) Immunoblot (upper panels) and quantitation (lower panels) of mitochondrial Aqp8bb in untreated or Ca^{2+} and/or H_2O_2 treated cells in the presence of BIM-II, SP600125 and CHIR99021 inhibitors. (F) Immunoblot of kinase activation (upper panels) and corresponding quantitation (lower panels) in cells treated as in E. In C-F, data (mean \pm SEM; $n = 3$ separate experiments) are statistically analyzed by one-way ANOVA. *** $P <$

0.001; ** $P < 0.01$; * $P < 0.05$, with respect to non-treated cells, or as indicated in brackets. (G) Summarized model of the pathways activated in HepG2 cells controlling Aqp8bb mitochondrial transport.

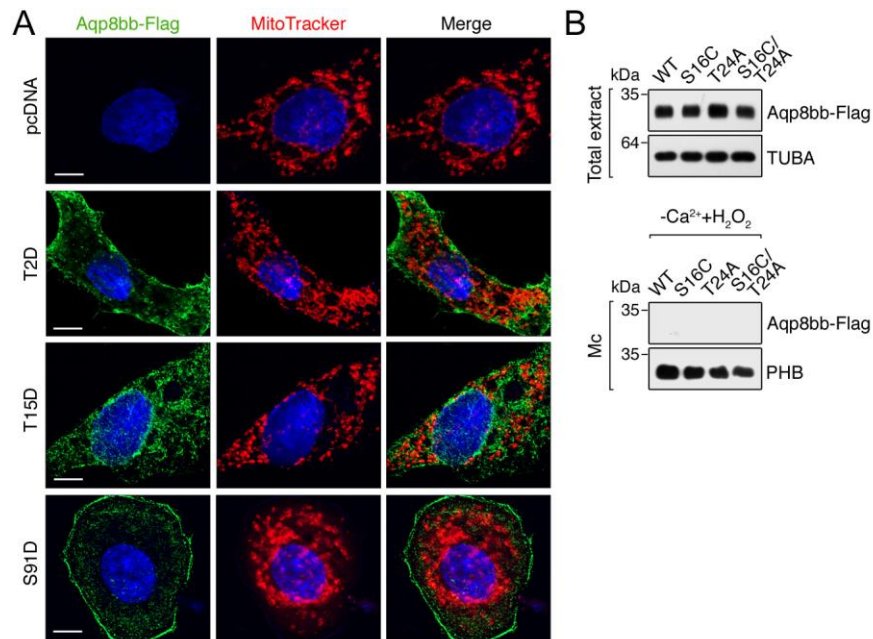


Fig. S9. Effect of seabream Aqp8bb mutants on mitochondrial channel transport in HepG2 cells. (A) Double staining of Aqp8bb-Flag (green) and mitochondria (MTR, red) in cells transfected with empty pcDNA vector or transiently expressing Aqp8bb-Flag-T2D, -T15D or -S91D. Scale bars, 10 μ m. (B) Upper panels, immunoblot of Aqp8bb-Flag-WT and channel mutants preventing Ser¹⁶ and Thr²⁴ phosphorylation, or both, in total protein extracts from HepG2 cells. Tubulin (TUBA) is used as loading control. Lower panels, immunoblot of the same constructs in mitochondrial extracts (Mc), using PHB as control, from cells not exposed to Ca²⁺ and H₂O₂. Molecular mass markers are on the left.

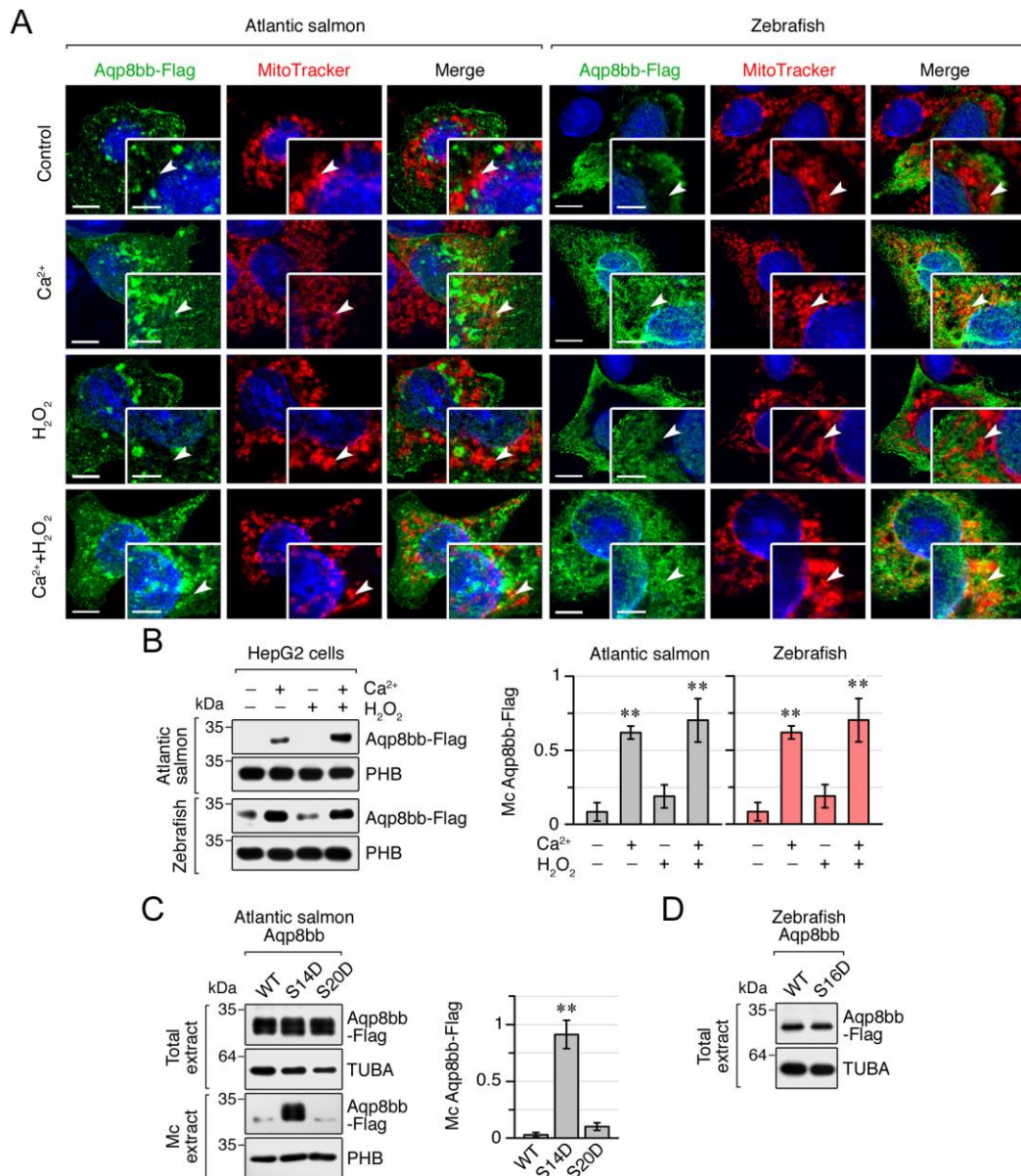


Fig. S10. Transient expression of Atlantic salmon and zebrafish Aqp8bb-Flag in HepG2 cells. (A) Double staining of salmon or zebrafish Aqp8bb-Flag (green) and mitochondria (MTR, red) in non-treated HepG2 cells or after external treatment with Ca²⁺ (10 mM) and/or H₂O₂ (100 μM). The arrowheads indicate co-localized signals. Scale bars, 10 μm (insets 5 μm). (B) Representative immunoblot of mitochondrial Aqp8bb-Flag (left panels), and corresponding quantitation normalised to PHB (right panels), from HepG2 cells transiently expressing salmon or zebrafish Aqp8bb-Flag-WT and exposed to Ca²⁺ and/or H₂O₂. (C) Immunoblot of salmon Aqp8bb-Flag-WT and the Aqp8bb-Flag-S14D and -S20D mutants in HepG2 cells. The left upper panels show the expression of the different channels and tubulin (TUBA), whereas the left lower panels show the accumulation of the constructs in the mitochondria. On the right, is depicted the corresponding mitochondrial quantitation normalised to PHB. Data (mean ± SEN; n = 3 separate experiments) in B and C are statistically analyzed by one-way ANOVA. **P < 0.001, with respect to untreated cells (B) or salmon Aqp8bb-Flag-WT (C). (D) Immunoblot showing the expression levels of total zebrafish Aqp8bb-Flag-WT and the Aqp8bb-Flag-S16D mutant, and of TUBA, in HepG2 cells.

Supplementary Materials and Methods

Animals and sperm collection. Adult gilthead seabream males were raised in captivity at Institut de Recerca i Tecnologia Agroalimentàries (IRTA) aquaculture facilities in San Carlos de la Ràpita (Tarragona, Spain) and maintained in the laboratory as previously described (1). Zebrafish and Atlantic salmon were maintained, respectively, at the PRBB Animal Facility (Barcelona, Spain) and the Matredal Aquaculture Research Station (Norway). In seabream and salmon, milt was recovered by abdominal massage from sedated males, whereas sperm were collected from zebrafish by surgical removal of the testis from anesthetized males. Procedures relating to the care and use of animals and sample collection were approved by the Ethics Committee (EC) of IRTA, following the European Union Council Guidelines (86/609/EU), or in accordance with the regulations approved by the governmental Norwegian Animal Research Authority (<http://www.fdu.no/fdu/>).

Reagents and antibodies. The drugs, enzymes and other compounds used for the different experiments in this study are listed in Table S1, whereas commercial and custom made antibodies employed are described in Table S2. Other reagents were purchased from Merck unless indicated otherwise.

DNA constructs. Full-length cDNAs encoding seabream, Atlantic salmon and zebrafish wild-type Aqp8bb (GenBank accession Nos. DQ889225.1, KC626880.1 and FJ695516.2, respectively), which were Flag-tagged at the N-terminus by PCR, were subcloned into the pcDNA3 expression vector. Plasmids encoding dominant-negative forms of human JNK, Jnk1a1(apf) (plasmid # 13846), and *Xenopus laevis* GSK3, pCS2 DN-GSK3-GFP (plasmid # 29681), were purchased from Addgene. Site-directed mutagenesis was carried out using the QuikChange Lightning Site-Directed Mutagenesis Kit (Agilent Technologies). Oligonucleotides were ordered from Thermo Fisher Scientific and constructs were verified by DNA sequencing (Macrogen).

Computational analysis of aquaporin structure. Prediction of kinase-specific phosphorylation residues in seabream, Atlantic salmon and zebrafish Aqp8bb orthologs was carried out using the NetPhos 3.1 Server (<http://www.cbs.dtu.dk/services/NetPhos/>) (2) and The Eukaryotic Linear Motif resource (<http://elm.eu.org/>) (3). The three-dimensional structures of the seabream Aqp8bb were built as described previously (4) using the model leverage option in the modeller server (modbase.compbio.ucsf.edu), based upon the *Pichia pastoris* Aqy1 (3GD8) template. The best scoring model was selected using the slow (Seq-Prf, PSI-BLAST) assignment method and rendered with MacPymol (pymol.org).

Sperm treatments and evaluation of motility by CASA. Freshly ejaculated sperm from seabream and salmon was diluted 1:100 in NAM (in mg/ml: 3.5 NaCl, 0.11 KCl, 1.23 MgCl₂, 0.39 CaCl₂, 1.68 NaHCO₃, 0.08 glucose, 1 bovine serum albumine [BSA], pH 7.7; 280 mOsm) (1), or in non-activating diluent 1 (5), using BSA instead of L- α -lecithin (in mg/ml: 8 NaCl, 0.82 KCl, 0.57 Na₂HPO₄, 4 BSA, pH 8; 300 mOsm), respectively. For zebrafish, sperm was isolated by crushing or dissecting the testis in the non-activating SS300 solution (in mg/ml: 8.15 NaCl, 0.67 KCl, 0.11 CaCl₂, 0.12 MgSO₄, 0.18 glucose, 2.42 Tris-Cl pH 8.0; 300 mOsm) (6) followed by a gentle centrifugation (100 × g). Spermatozoa concentration was determined by CASA using the Integrated Semen Analysis System (ISASv1, Proiser) software as previously described (1). In all species, sperm (10⁹ cells/ml in the corresponding NAM) was treated with increasing concentrations of the different kinase inhibitors/activators (0.1, 1, 5 and 10 μ M, or with one 10 μ M dose), or the vehicle (0.5% DMSO; controls), for 1 h (seabream and salmon) or 15 min (zebrafish) at room temperature, and subsequently activated by 1:10 (seabream and salmon) or 1:3 (zebrafish) dilution in filtered SW

(seabream) or deionized water (salmon and zebrafish) for 5 s. The effect of Ca^{2+} or ROS on immotile spermatozoa was tested by exposing NAM-incubated sperm to 10 μM of the different kinase inhibitors for 30 min, and subsequently treated with 3 mM CaCl_2 and 10 μM of the Ca^{2+} ionophore A23187 (7), or increasing doses of X-XO (X-XO1: 0.1 mM X + 0.01 U/ml XO; X-XO2: 0.2 mM X + 0.0175 U/ml XO; X-XO3: 0.3 mM X + 0.025 U/ml XO) (8), for another 30 min. In some experiments, seabream sperm was activated in SW in the presence of increasing doses of BAPTA (5, 50 and 500 μM) and/or DPI (1, 5 and 50 μM). For seabream and zebrafish, the percentage of total motile and progressive spermatozoa and VCL, in the presence or absence of kinase inhibitors, were recorded by CASA every 10 s up to 3 min at room temperature (Table S3).

Cell culture. Human embryonic kidney cells 293T (HEK293T, ATCC # CRL-11268) and Hepatocellular carcinoma HepG2 cells (ATCC # CRL-10741) were grown at 37°C in an atmosphere of air/ CO_2 [95:5 (v/v)] in Dulbecco's modified Eagle's medium (DMEM) supplemented with 10% v/v fetal bovine serum (FBS), 260 U/ml of penicillin and streptomycin, and 2 mM L-glutamine. At 75% of confluence, cells were transiently transfected in 6-well plates with 5 μg of WT Aqp8bb-Flag and/or 5 μg of the desired constructs, or with 5 μg of the pcDNA3 vector alone, using Lipofectamine 3000 (Invitrogen). The following day, the cells were trypsinized and used for the different experiments. To test the effect of Ca^{2+} and/or H_2O_2 on Aqp8bb trafficking, HepG2 cells were preincubated or not with kinase inhibitors for 1 h at 37°C and subsequently exposed to increasing doses of CaCl_2 (1, 5 or 10 mM) or H_2O_2 (20, 50, 100 or 200 μM) for 30 min.

Reverse transcriptase-PCR (RT-PCR). Total RNA was extracted from different adult tissues, including testis and sperm, using the RNeasy Minikit (Qiagen) including DNaseI treatment, following the manufacturer's instructions. Total RNA (5 μg) was reverse transcribed using 0.5 μg oligo(dT)₁₇ primer, 1 mM deoxynucleotide triphosphates (dNTPs), 40 IU RNase out (Life Technologies Corp.), and 10 IU SuperScript II Reverse Transcriptase enzyme (Life Technologies Corp.) for 1.5 h at 42°C. The PCR was carried out with 1 μl of the RT reaction in a final volume of 50 μl containing PCR buffer, 0.2 mM dNTPs, 1 IU of Taq polymerase (Roche), and 1 μM of forward and reverse primers (Table S4 and Fig. S2A). Reactions were amplified using one 5-min cycle of 95°C; 35 cycles of 95°C for 30 sec, 60°C for 30 sec, and 72°C for 1 min; and a final 7-min elongation at 72°C. PCR products were run on 1% agarose gels and photographed.

Functional expression in *Xenopus laevis* oocytes. Full-length zebrafish Aqp8bb-M1 and -M22 cDNAs were subcloned into the pT7Ts vector for expression in *X. laevis* oocytes (9). The cRNAs for microinjection of oocytes were synthesized with T7 RNA polymerase plus (Ambion) from *Xba*I-linearized plasmids. Isolation of stage V oocytes and microinjection was performed as previously described (9). Oocytes were transferred to modified Bart's solution (MBS; 88 mM NaCl, 1 mM KCl, 2.4 mM NaHCO_3 , 0.82 mM MgSO_4 , 0.33 mM $\text{Ca}(\text{NO}_3)_2$, 0.41 mM CaCl_2 , 10 mM HEPES, and 25 $\mu\text{g}/\text{ml}$ gentamycin, pH 7.5) and injected with 50 nl of distilled water (negative control) or 50 nl of water solution containing 5ng of Aqp8bb-M1 or -M22 cRNA. One day after injection, oocytes were manually defolliculated and subsequently maintained in MBS at 18°C. The osmotic water permeability (P_f) was determined the following day by transferring the oocytes into 10-fold diluted MBS (20 mOsmol) and oocyte swelling was recorded by video microscopy using serial images at 2 sec intervals during the first 20 sec using a Nikon Color view video camera coupled to a stereomicroscope (SMZ1000, Nikon Corp., Tokyo, Japan). The P_f values were calculated taking into account the time-course changes in relative oocyte volume ($d(V/V_0)/dt$), the molar

volume of water ($V_w = 18 \text{ cm}^3/\text{ml}$) and the oocyte surface area (S) using the formula $V_0(d(V/V_0)/dt)/(SV_w(Osm_{in} - Osm_{out}))$.

Determination of $[Ca^{2+}]_i$ and ROS Levels. Intracellular Ca^{2+} content in sperm was estimated using the Fluo-3-AM vital dye. Motile and immotile sperm (10^9 cells/ml), previously incubated in the presence or absence of selected drugs for 1 h, were loaded during the last 15 min with a 1:200 diluted solution containing equivalent volumes (1:1) of 1 mM Fluo3-AM in DMSO and 8% NP-40 in 20% DMSO (5 μM Fluo3-AM and 0.3% DMSO final). In some experiments, 10 μM of the Ca^{2+} ionophore A23187 was added at the end of the incubation period for 1 min as above. Sperm were then centrifuged at $1000 \times g$ for 1 min and resuspended in fresh NAM. A 15- μl aliquot of the sperm suspension was loaded in each well (10^7 cells/well) of a black 96-well microplate (Nunc F96 MicroWell Black and White Polystyrene Plate; Thermo Fisher Scientific Inc.) and diluted with 135 μl of either NAM or SW for 5 min prior to measurement of the fluorescence intensity at excitation and emission wavelengths of 506 and 526 nm, respectively, using an Infinite M200 microplate reader (Tecan Group Ltd.). The background signal of sperm in NAM or SW not loaded with Fluo3-AM was subtracted from each value.

For ROS determination, sperm cells were loaded with 200 mM of the CM- H_2 DCFDA dye for 1 h, during which drugs were added as described above. Sperm was centrifuged 1 min at $1000 \times g$, and resuspended in fresh NAM to wash out the dye. Aliquots of 10 μl were loaded in 96-well plates and diluted 1:10 in NAM or SW prior to measurement of fluorescence intensity as above. The background signal of non-loaded sperm sperm was also subtracted to each value. The same protocols were used to measure Ca^{2+} and ROS in HepG2 cells plated in 96-well plates. In all cases, measurements were carried out in triplicate or quadruplicate.

Isolation of mitochondria from sperm and cultured cells. For mitochondria isolation from spermatozoa, sperm (10^{10} cells/ml) was treated with 250 ng/ml MitoTracker Red and kinase modulators for 1 h, and centrifuged at $700 \times g$ during 5 min at room temperature. The pellet was then resuspended in 400 μl of either NAM or SW and the heads and flagellum of spermatozoa were immediately separated by passing the sperm extract 10 times through a capillary (0.5 mm diameter) attached to a 2-ml syringe. The suspension was then placed on top of a sucrose gradient prepared in 2-ml microtubes (400 μl of 2 M sucrose, then 400 μl of 1.5 M sucrose, 400 μl of 1 M sucrose, and finally 400 μl of 0.5 M sucrose), and centrifuged at $14000 \times g$ for 60 min at 4°C . Heads containing mitochondria stained in red were recovered with a micropipette at the 2 M-1.5 M interface (approximately 250 μl) and diluted in 1.25 ml of 0.9% NaCl before centrifuging at $10000 \times g$ for 15 min at 4°C . The pellet was resuspended by pipetting up and down 5 times in 200 μl of the mitochondria homogenization buffer (MHB: 10 mM Tris-HCl pH 7.5, 10 mM KCl, 0.15 mM $MgCl_2$, 1 mM DTT, 1 mM NaF, 1 mM Na_3VO_4 , and protease inhibitors [EDTA-free Protease Inhibitor Cocktail Tablets]) and kept on ice for 10 min. Subsequently, 30 μl of 2 M sucrose was added to the extract (to obtain a final concentration of 0.25 mM sucrose) and the suspension was gently vortexed and centrifuged at $1200 \times g$ for 5 min at 4°C . The supernatant was transferred to a new 1.5-ml microtube and centrifuged again at $1200 \times g$ for 5 min at 4°C . Finally, the supernatant was transferred to a new 1.5-ml tube and centrifuged at $7000 \times g$ for 10 min at 4°C . The resulting pellet was resuspended in 100 μl of the mitochondria resuspension buffer (MRB: 10 mM Tris-HCl pH 6.7, 0.15 mM $MgCl_2$, 0.25 mM sucrose, 1 mM DTT, 1 mM NaF, 1 mM Na_3VO_4 , plus protease inhibitors) and centrifuged at $9500 \times g$ for 5 min at 4°C . The final mitochondrial pellet was used for H_2O_2 uptake assays (see below), the isolation of inner mitochondrial membranes as previously described (10), or immunoblotting. For the later, the pellet was resuspended in 50 μl of PBS plus protease inhibitors, phosphatase inhibitor cocktail 2, 1 mM NaF, and 1 mM Na_3VO_4 . The protein content was measured with a

NanoDrop 2000c spectrophotometer and the volume adjusted to obtain a concentration of 2.5 µg protein/µl. Then, the sample was mixed with 2 × Laemmli sample buffer plus 0.1 M DTT, and boiled at 95°C for 10 min before freezing in liquid nitrogen and storage at -80°C until Western blot analysis.

Mitochondria from HepG2 cells were isolated after 1 h incubation at 37°C with MitoTracker Red, with or without kinase inhibitors and in the presence/absence of CaCl₂ and/or H₂O₂. DMEM media was replaced in each of the 6-well plate with 1 ml of lysis buffer (10 mM NaCl, 1.5 mM MgCl₂, 10 mM Tris HCl, pH 7.5, 1 mM DTT) and cells were mixed using a shaker during 5 min in order to break their membranes and detach them from the plate. Cells were then scrapped and the resulting suspension was homogenized with a syringe before adding 1 ml of 2 × homogenization buffer (210 mM mannitol, 70 mM sucrose, 5 mM Tris-HCl, pH 7.5, 10 mM HEPES pH 7.5, and 1 mM EDTA). The extract was transferred to a 2-ml microtube and cellular debris were pelleted by three times centrifugation at 1200 × g for 5 min at 4°C. The supernatant containing the mitochondrial extract was centrifuged at 10000 × g for 10 min at 4°C. The mitochondrial pellet was resuspended in 1 × Laemmli sample buffer containing 0.1 M DTT, and immediately heated at 95°C for 10 min.

Mitochondrial H₂O₂ uptake. The mitochondria extracted from spermatozoa as described above were tested for H₂O₂ uptake using 300 µM of external H₂O₂ as previously described (10). Measurements were carried out in triplicate.

Protein extraction from sperm and cultured cells. Sperm (10⁹ cell/ml) were centrifuged for 1 min at 1000 × g and the pellet immediately resuspended in a kinase extraction buffer (50 mM Tris/HCl pH 7.5, 150 mM NaCl, 1% Triton X100, 1% sodium deoxycholate, 1 mM EGTA, 0.4 mM EDTA, 1 mM Na₃VO₄, 1 mM NaF, and protease inhibitors), vortexed for 1 min, and kept on ice for 5 min. After sonication at 15% amplitude for 5 s and centrifugation at 14000 × g for 10 min at 4°C, the supernatant was removed and its protein concentration was measured by Bradford and adjusted to 6 µg protein/µl. The supernatant was then mixed with 4 × Laemmli sample buffer with DTT supplemented with protease inhibitors, 2 mM Na₃VO₄, and 2 mM NaF, and 4 × phosphatase inhibitor cocktail 2, to obtain a final concentration of 4 µg protein/µl. Samples were heated at 95°C for 10 min, frozen in liquid nitrogen and stored at -80°C until immunoblotting.

For protein extraction from HepG2 cells, transfected cells grown in six-well plates were trypsinized and transferred to a 1.5-ml microtube and centrifuged at 500 × g for 5 min. The pellet was resuspended in 1 ml of radioimmunoprecipitation assay (RIPA) buffer (150 mM NaCl, 50 mM Tris pH 8.0, 1.0% Triton X-100, 0.5% sodium deoxycholate, 0.1% SDS, supplemented with 1 mM NaF, 1 mM Na₃VO₄, protease inhibitors, and 80 U benzonase), vortexed, and incubated for 5 min on ice. The samples were centrifuged at 14000 × g at 4°C for 2 min, and the supernatant was mixed with 2 × Laemmli sample buffer with DTT and heated at 95°C for 10 min. Samples were frozen and stored as indicated above.

Protein extraction of total membranes from *X. laevis* oocytes. Oocytes were homogenized in HbA buffer (20 mM Tris, pH 7.4, 5 mM MgCl₂, 5 mM NaH₂PO₄, 1 mM EDTA, 80 mM sucrose, and cocktail of protease inhibitors [Mini EDTA-free; Roche]) and total membranes were isolated as previously described (11).

Immunoprecipitation. HEK293T and HepG2 transfected cells were lysed in an immunoprecipitation buffer (50 mM Tris-HCl pH 7.4, 150 mM NaCl, 1 mM EDTA, 1 mM EGTA, 5 mM MgCl₂, 1 mM NaF, 1 mM Na₃VO₄, 0.5% Triton X-100, and protease inhibitors). An aliquot (10%) of the extract was collected as “input” and mixed with 2 × Laemmli + DTT supplemented with protease inhibitors, 2 mM Na₃VO₄, and 2 mM NaF. The remaining extract was mixed with activated G-protein beads (Pure Proteome™

Protein G Magnetic Beads) coupled to seabream Aqp8bb antibody or rabbit anti-Flag antibody, or rabbit IgG as negative control, following manufacturer's instructions, and incubated overnight at 4°C under constant agitation. The beads were further washed three times with PBST, eluted in 50 µl of RIPA buffer, and mixed with 4 × Laemmli supplemented with protease and phosphatase inhibitors.

In Vitro Phosphorylation Assays. Immunoprecipitation eluates from cultured cells were dissolved on ice with a kinase assay buffer (25 mM MOPS, pH 7.2, 12.5 mM β-glycerophosphate, 25 mM MgCl₂, 5 mM EGTA, 2 mM EDTA, 0.1 mM Na₃VO₄ and 0.25 mM DTT), and diluted 5-fold with a solution containing 50 ng/ml BSA, 200 µM ATP, and 50-400 ng (0.04-0.33 µM) of rGSK3β or 200 ng of rJNK1 (0.11 µM) or rPKCα (0.08 µM) (Table S1). The mixture was incubated 30 min at 30°C and the reaction terminated by adding Laemmli sample buffer and heating at 95°C for 10 min. Samples were subsequently processed for immunoblotting.

Immunoblotting. Laemmli-mixed protein samples were heated at 95°C for 10 min and subjected to 12% sodium dodecyl sulfate polyacrylamide gel electrophoresis (SDS-PAGE), and blotted onto Immun-Blot nitrocellulose 0.2 µm Membrane (Bio-Rad Laboratories), as previously described (1). Membranes were blocked with 5% nonfat dry milk or 3% BSA in TBST (20 mM Tris, 140 mM NaCl, 0.1% Tween, pH 8) for 1 h at room temperature, and subsequently incubated overnight at 4°C with the selected antibody diluted in TBST with 5% milk or 3% BSA as listed in Table S2. Bound antibodies were detected with horseradish peroxidase-coupled anti-mouse, rabbit or goat secondary antibodies (Table S2) diluted as above, and reactive protein bands were revealed using Immobilon™ Western chemiluminescent HRP substrate. For the semi-quantitative determination of Aqp8bb or kinase abundance in the mitochondria or total extracts, respectively, under the different treatments, the intensity of the immunoreactive bands was scored by densitometry using the Quantity-One software (Bio-Rad Laboratories Inc.), and normalized to that of the reference proteins prohibitin or alpha-tubulin. Quantitation of Ser and Thr phosphorylation of Aqp8bb-Flag was normalised to the total immunoprecipitated protein.

Immunofluorescence microscopy of sperm and cultured cells. Spermatozoa labelled with MitoTracker and treated as described above were attached to UltraStick/UltraFrost Adhesion slides (Electron Microscopy Sciences) at room temperature as previously described (1), fixed in 4% paraformaldehyde (PFA) for 5 min, and subsequently permeabilized using PBST (137 mM NaCl, 2.7 mM KCl, 100 mM Na₂HPO₄, 2 mM KH₂PO₄, pH 7.4, 0.1% Triton X-100) for 10 min. Slides were blocked in 5% normal goat serum plus 0.1% BSA in PBST for 1 h, and incubated with the antibodies at different dilutions (Table S2) overnight at 4°C in PBST. After washing, sections were incubated with the corresponding Alexa Fluor 488-conjugated secondary antibodies (Table S2) for 1 h at room temperature, washed in PBS, and counterstained with 4',6-diamidino-2-phenylindole (DAPI; 1:5000) for 3 min in PBS to stain the nuclei. The sections were mounted with fluoromount aqueous anti-fading medium, and examined and photographed with a Zeiss Axio Imager Z1/ApoTome fluorescence microscope (Carl Zeiss Corp.). Images from negative control sections were taken with the same fluorescence intensity and exposure times than those used for the positives. To determine the percentage of spermatozoa showing Aqp8bb mitochondrial localization, the number of spermatozoa displaying co-localization of Aqp8bb and MitoTracker signals was scored in at least 100 spermatozoa per ejaculate or pool.

For immunofluorescence microscopy on cultured cells, cells attached to round coverslips were fixed in methanol during 6 min at -20°C, and subsequently in acetone for 30 s. Cells were washed twice in PBS and then permeabilized with PBST for 10 min. The blocking step and incubation with primary and secondary antibodies was

carried out as described above, except that the counterstaining with DAPI was used at 1:3000 dilution for 10 min.

Immunofluorescence microscopy on testis sections. Zebrafish and Atlantic salmon testis explants, previously incubated for 1 h with 250 ng/ml MitoTracker® Red CMXRos (Invitrogen), were fixed in 4% paraformaldehyde (PFA) for 6 h, washed, dehydrated, and embedded in Paraplast Plus®. Sections (7 µm) were blocked in 5% goat serum and 0.1% BSA in PBS with 0.1% Tween-20 (PBST) for 1 h, and incubated with PBS containing 0.2% Triton X-100 for 10 min at room temperature. Incubation with the primary antibodies diluted in PBS (Table S2) was performed overnight at 4°C. Slides carrying adjacent sections of the testis were incubated with the antibodies previously adsorbed with the respective immunizing peptides as negative controls. After washing, sections were probed with an Alexa 488-coupled anti-rabbit IgG secondary antibody (Table S2) for 1 h at room temperature. The nuclei were counterstained with 4',6-diamidino-2'-phenylindole dihydrochloride (DAPI) and mounted with fluoromount aqueous anti-fading medium. Sections were examined and photographed with a Zeiss Axio Imager Z1/ApoTome fluorescence microscope (Carl Zeiss Corp.).

Statistics. Results are expressed as the means ± SEM. For seabream and salmon sperm, experiments were carried out on three to eight different males (one ejaculate per male), whereas in the case of zebrafish, experiments were done on five to seven males or on three pools each containing sperm from five different males. Sperm kinetics analysis by CASA were run in triplicate for each ejaculate/pool. For cultured cells, data were obtained from three independent experiments. Comparisons between two independent groups were made by the two-tailed unpaired Student's *t*-test. The statistical significance among multiple groups was analyzed by one-way ANOVA, followed by the Tukey's multiple comparison test, or by the non-parametric Kruskal-Wallis test and further Dunn's test for nonparametric post hoc comparisons, as appropriate. Time-course curves of sperm kinetic parameters were compared by the Mann-Whitney *U* test. Percentages were square root transformed previous analyses. Statistical analyses were carried out using the SigmaPlot software v12.0 (Systat Software Inc.) and GraphPad Prism v8.4.3 (686) (GraphPad Software). In all cases, statistical significance was defined as $P < 0.05$ (*), $P < 0.01$ (**), or $P < 0.001$ (***)

Table S1. Drugs, enzymes and other compounds used for the different experiments in this study

Compound	Abbreviation	Vendor	Catalog no.	Activity
Anisomycin	ANS	Merck	A9789	Inducer of JNK and p38 MAPK phosphorylation
1,2-Bis(2-Aminophenoxy)ethane-N,N,N',N'-tetraacetic acid	BAPTA	Invitrogen	B6769	Cell-permeant chelator, highly selective for Ca ²⁺
Bisindolylmaleimide II	BIM-II	Santa Cruz Biotechnology	sc-221366	ATP-competitive PKC subtypes inhibitor
Calcium Ionophore A23187	A23187	Merck	C7522	Increases the ability of Ca ²⁺ to cross biological membranes
Calphostin C	Cal-C	Santa Cruz Biotechnology	sc-3545	Inhibitor of PKC that targets the regulatory domain
CHIR99021	CHIR99021	Merck	SML1046	Inhibitor of GSK3 kinetic activity
CM-H ₂ DCFDA	DCFDA	Molecular Probes	C6827	Indicator for ROS in cells
Diphenyleneiodonium chloride	DPI	Merck	D2926	Inhibitor of NADPH oxidase
Doramapimod	BIRB796	Selleck Chemicals	S1574	Inhibitor of kinetic activity and phosphorylation of p38 MAPK
Fluo-3, AM	Fluo-3-AM	Invitrogen	F14218	Cell permeable Ca ²⁺ indicator
GNF-7	GNF-7	Merck	SML1501	Ras signaling inhibitor; inhibits Ack1 and GCK
H-89 dihydrochloride hydrate	H-89	Merck	B1427	ATP-competitive PKA inhibitor
IgG from rabbit serum	IgG	Merck	I5006	Immunoglobulin G
Mito-TEMPO	-	Santa Cruz Biotechnology	sc-221945	Mitochondria-targeted antioxidant
MitoTracker TM Red CMXRos	MTR	Molecular Probes	M-7512	Mitochondria-specific, red-fluorescent dye
MK-2206 dihydrochloride	MK2206	Selleck Chemicals	S1078	Allosteric inhibitor of AKT, and activator of GSK3
NG25 trihydrochloride	NG25	Merck	SML1332	ATP-competitive TAK1 and GSK3 inhibitor
NQDI 1	NQDI-1	Tocris Bioscience	4429	ASK1 inhibitor
PD 98,059	PD98059	Merck	P215	Inhibitor of MEK/MKK phosphorylation
Phorbol 12-myristate 13-acetate	PMA	Merck	P8139	Analog of diacylglycerol, the physiological activator of PKC
4 α -Phorbol 12-myristate 13-acetate	4 α -PMA	Merck	P148	Negative control for PMA activation of PKC
Recombinant JNK1	rJNK1	Merck	J2455	JNK1 active, GST tagged from mouse
Recombinant GSK3 β	rGSK3 β	Merck	G4296	GSK3 β active, His tagged from human
Recombinant PKC- α	rPKC α	Merck	SRP5251	PKC- α active, GST tagged from <i>Xenopus</i> sp.
SB 202190	SB202190	Merck	S7067	ATP-competitive p38 MAP kinase inhibitor
SH-5	SH-5	Santa Cruz Biotechnology	sc-205973	Inhibitor of AKT activation
SP 600125	SP600125	Merck	S5567	ATP-competitive JNK inhibitor
Xanthine	X	Merck	X4002	Purine base
Xanthine Oxidase	XO	Merck	X1875	Generates ROS following the oxidation of xanthine

Table S2. Antibodies used in this study

Antibody/UniProt accession no.	Host species	Vendor	Catalog no.	Working dilution ^a		
				IB	IF	IP
Seabream Aqp8bb/C7S301	Rabbit	Custom made (1)	-	1:1000	1:500	1:500
Atlantic salmon Aqp8aa/S5RRC8	Rabbit	Custom made (12)	-	1:1000	-	-
Atlantic salmon Aqp8ab/S5R5I0	Rabbit	Custom made (12)	-	1:1000	-	-
Atlantic salmon Aqp8bb/C0HB60	Rabbit	Custom made (12)	-	1:1000	1:400	-
Zebrafish Aqp8bb/D3U0R1	Rabbit	Custom made, this study ^b	-	1:1000	1:400	-
ASK/Q99683	Rabbit	Signalway Antibody	21134	1:1000	-	-
ASK1(pS ⁹⁶⁶)/Q99683	Rabbit	Signalway Antibody	11179	1:1000	-	-
Flag, clone M2	Mouse	Merck	F3165	1:1000	1:1000	1:500
Flag	Rabbit	Merck	F7425	1:1000	1:1000	1:500
GSK3a/b/ P49840,P49841	Mouse	Santa Cruz Biotechnology	sc-7291	1:1000	-	-
GSK3a/b (pY ^{279/216})/P49840,P49841	Rabbit	Signalway Antibody	11301	1:1000	-	-
GSK3a (pS ²¹)/ P49840	Rabbit	Signalway Antibody	11007	1:500	-	-
GSK3b (pS ⁹)/ P49841	Mouse	Santa Cruz Biotechnology	sc-373800	1:500	-	-
JNK (JNK1/3)/ P45983	Goat	Santa Cruz Biotechnology	sc-474	1:1000	-	-
JNK1/2/3(pT ¹⁸³ /Y ¹⁸⁵)/ P45983,P45984,P53779	Mouse	Santa Cruz Biotechnology	sc-6254	1:200	-	-
MEK-4/P45985	Rabbit	Signalway Antibody	41138	1:500	-	-
MEK-4 (pT ²⁶¹)/ P45985	Rabbit	Signalway Antibody	12208	1:500	-	-
Phosphoserine (5B12)	Mouse	Signalway Antibody	12828	1:500	-	-
Phosphothreonine (H-2)	Mouse	Santa Cruz Biotechnology	sc-5267	1:500	-	-
Prohibitin/Q7T1D8	Rabbit	GeneTex	GTX124491	1:2000	-	-
Rabbit IgG Horseradish Peroxidase	Goat	Bio-Rad	172-1019	1:5000	-	-
Mouse IgG Horseradish Peroxidase	Goat	Bio-Rad	172-1011	1:5000	-	-
Goat IgG Horseradish Peroxidase	Rabbit	Merck	A8919	1:5000	-	-
Rabbit IgG Alexa Fluor 488	Goat	Invitrogen	A-11008	-	1:1000	-
Mouse IgG Alexa Fluor 488	Goat	Invitrogen	A-11001	-	1:1000	-
α-Tubulin, clone DM1A/F1NW97	Mouse	Merck	T9026	1:25000	-	-

^a IB: immunoblotting; IF: immunofluorescence; IP: immunoprecipitation.

^b A rabbit polyclonal antisera for zebrafish Aqp8bb is raised against a synthetic peptide, LGDNDTRVVMK, corresponding to the C-terminus amino acid residues of the corresponding predicted protein (Agrisera AB, Vännäs, Sweden). The antiserum is purified by affinity chromatography against the synthetic peptide, and its specificity is confirmed by ELISA, and by heterologous expression of the Aqp8bb protein in *Xenopus laevis* oocytes.

Table S3. Settings of the CASA system

Parameters for sperm tracking	Settings
Counting chamber	ISAS R2C10
Camera	ISAS 782C
Frames	25 frames per s
Image resolution	768 x 576 pixels
Magnification	× 20 phase
Particle area	0-30 µm
Connectivity ^a	14 µm
Cuvilinear velocity (VCL)	>10 µm/s
Path straightness (STR)	>10%
Linearity (LIN)	>10%
Wobble (WOB)	>10%
Max. velocity (for tracking)	500 µm/s
Average path velocity (VAP)	>10 µm/s

^a Connection of the sperm head tracks within different frames.

Table S4. RT-PCR primers for Atlantic salmon *aqp8aa*, *-8ab* and *-8bb* paralogs

Transcript	GenBank accession no.	Direction	Primer (5' to 3')
<i>aqp8aa</i>	KC626878	Forward	CAAAGACGGAGCTCTTCACC
		Reverse	CTGACGCACACACTCACAGA
<i>aqp8ab</i>	KC626879	Forward	CGGCGTTTACTATCCTCCAA
		Reverse	TCCACAGTGACTIONTGCATAGGA
<i>aqp8bb</i>	KC626880	Forward	CCCTGCTGCAATCACAAGAT
		Reverse	CAACAGCGGTAATCTCAGACC

SI References

1. F. Chauvigné, M. Boj, S. Vilella, R. N. Finn, J. Cerdà, Subcellular localization of selectively permeable aquaporins in the male germ line of a marine teleost reveals spatial redistribution in activated spermatozoa. *Biol. Reprod.* **89**, 37 (2013).
2. N. Blom, T. Sicheritz-Ponten, R. Gupta, S. Gammeltoft, S. Brunak, Prediction of post-translational glycosylation and phosphorylation of proteins from the amino acid sequence. *Proteomics* **4**, 1633-1649 (2004).
3. M. Gouw, S. Michael, H. Sámano-Sánchez, M. Kumar, A. Zeke *et al.*, The eukaryotic linear motif resource - 2018 update. *Nucleic Acids Res.* **46**, D428-D434 (2018).
4. F. Chauvigné, O. Yilmaz, A. Ferré, P. G. Fjellidal, R. N. Finn *et al.*, The vertebrate Aqp14 water channel is a neuropeptide-regulated polytransporter. *Commun. Biol.* **2**, 462 (2019).
5. R. K. Gallant, G. F. Richardson, M. A. McNiven, Comparison of different extenders for the cryopreservation of Atlantic salmon spermatozoa. *Theriogenology* **40**, 479-486 (1993).
6. J. L. Matthews, J. M. Murphy, C. Carmichael, H. Yang, T. Tiersch *et al.*, Changes to extender, cryoprotective medium, and *in vitro* fertilization improve zebrafish sperm cryopreservation. *Zebrafish* **15**, 279-290 (2018).
7. M. Boj, F. Chauvigné, J. Cerdà, Coordinated action of aquaporins regulates sperm motility in a marine teleost. *Biol. Reprod.* **93**, 40 (2015).
8. M. Hagedorn, M. McCarthy, V. L. Carter, S. A. Meyers, Oxidative stress in zebrafish (*Danio rerio*) sperm. *PLoS One* **7**, e39397 (2012).
9. Deen, P. M. T. *et al.* Requirement of human renal water channel aquaporin-2 for vasopressin-dependent concentration of urine. *Science* **264**, 92-95 (1994).
10. F. Chauvigné, M. Boj, R. N. Finn, J. Cerdà, Mitochondrial aquaporin-8-mediated hydrogen peroxide transport is essential for teleost spermatozoon motility. *Sci. Rep.* **5**, 7789 (2015).
11. Kamsteeg, E. J. & Deen, P. M. Detection of aquaporin-2 in the plasmamembranes of oocytes: a novel isolation method with improved yield and purity. *Biochem. Biophys. Res. Commun.* **282**, 683-690 (2001).
12. Engelund, M.B., Chauvigné, F., Christensen, B.M., Finn, R.N. Cerdà, J. & Madsen, S.S. Differential expression and novel permeability properties of three aquaporin 8 paralogs from seawater-challenged Atlantic salmon smolts. *J. Exp. Biol.* **216**, 3873-3885 (2013).